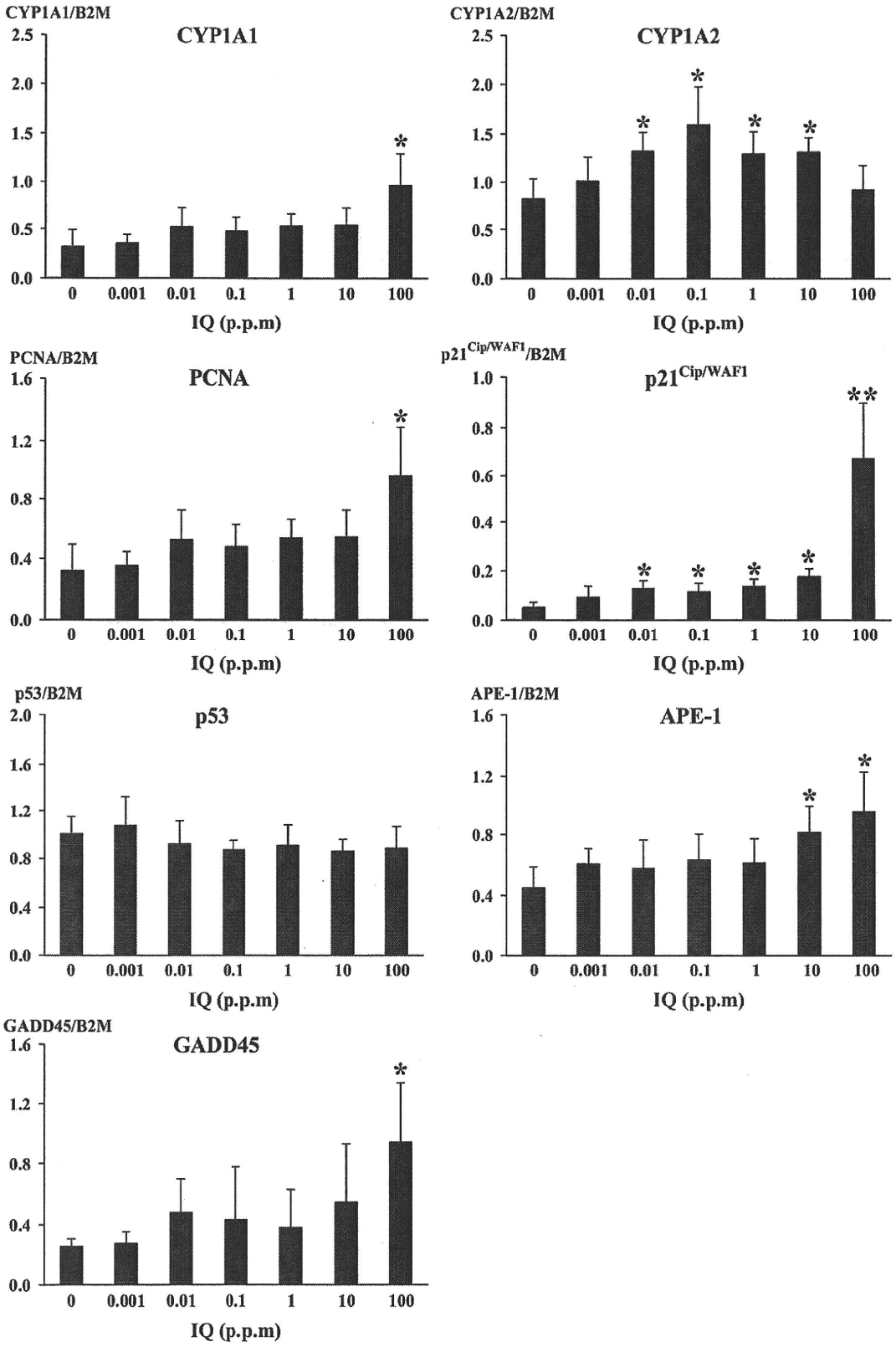

Fig. 2. Relative mRNA expression in the livers of rats at week 16. *Significantly different from 0 p.p.m. **Significantly different from all other groups. APE-1, AP endonuclease-1; B2M, beta-2-microglobulin; GADD45, growth arrest and DNA damage-inducible protein 45; PCNA, proliferating cell nuclear antigen.

doi: 10.1111/j.1349-7006.2010.01761.x

Table 4. Development of ACF in the colons of rats administered IQ for 16 weeks

Group	IQ (p.p.m.)	No. rats	Size of ACF				
			1	2	3	≥4	Total
1	0	240	0.08 ± 0.28	0.12 ± 0.32	0.06 ± 0.25	0.08 ± 0.29	0.33 ± 0.64
2	0.001	240	0.12 ± 0.36	0.08 ± 0.29	0.10 ± 0.32	0.09 ± 0.30	0.39 ± 0.69
3	0.01	240	0.15 ± 0.41	0.15 ± 0.42	0.06 ± 0.24	0.06 ± 0.24	0.43 ± 0.77
4	0.1	240	0.11 ± 0.33	0.11 ± 0.35	0.06 ± 0.25	0.08 ± 0.27	0.36 ± 0.63
5	1	240	0.15 ± 0.45	0.10 ± 0.30	0.10 ± 0.33	0.05 ± 0.23	0.41 ± 0.80
6	10	240	0.19 ± 0.48*	0.16 ± 0.41	0.07 ± 0.25	0.09 ± 0.40	0.50 ± 0.86
7	100	120	1.48 ± 1.46*	1.29 ± 1.51*	0.70 ± 0.93*	0.72 ± 1.01*	4.19 ± 3.34*

*Significantly different from group 1. ACF, aberrant crypt foci; IQ, 2-amino-3-methylimidazo[4,5-f]quinoline.

not induce CYP1A1. Therefore, it is reasonable to postulate that the dose-relationship between IQ and induction of CYP1A1 is not a simple dose-response. CYP1B1 does not appear to be involved in the metabolism of IQ at doses up to 100 p.p.m. in rats. The findings described above demonstrate the importance of taking into account dosage, duration and route of exposure in interpretation of the data on metabolic activation of IQ. Further studies on the dose-response relationships between chronic IQ exposure and the protein expression levels and activities of detoxifying enzymes, especially at doses relevant to human exposure, would provide further insight into the role of metabolic activation in IQ carcinogenicity.

Oxidative DNA damage does not appear to play a role in IQ-induced carcinogenesis. In the present study, no significant changes in 8-OHdG levels or Ogg1 expression levels in the livers of IQ-treated rats were observed. Our results are consistent with the recent findings in IQ-treated Big Blue rats that oxidative stress was not responsible for the initiation of IQ-induced carcinogenesis in the liver and colon.[37] In this respect, IQ is different from MeIQx, in which oxidative DNA damage plays an important role in liver carcinogenesis.[48]

In summary, the present study provides the first experimental data on the carcinogenicity of low doses of IQ in both the liver and colon of the test animal and compares the effect of IQ at the cellular level with its carcinogenic effect. Our findings support the idea that there is a practical threshold that should be considered when evaluating the risk of genotoxic carcinogens. To this end, further accumulation of data, especially mechanistic data, should be promoted to facilitate not only an understanding of the carcinogenic effects of low doses of genotoxic carcinogens but also to establish an accurate means of quantitative risk assessment.

Acknowledgments

The authors would like to acknowledge the encouragement of Dr N. Ito (Emeritus Professor, Nagoya City University Medical School, Nagoya, Japan) and Dr T. Kitagawa (Emeritus Director, the Cancer Institute of Japanese Foundation for Cancer Research, Tokyo). This research was supported by a grant from the Japan Science and Technology Corporation, included in the Project of Core Research for Evolutional Science and Technology (CREST) and a Grant-in-Aid for Specially Promoted Research from the Ministry of Education, Science, Sports, Culture and Technology of Japan.

Disclosure Statement

The authors have no conflict of interest.

References

1 Wakabayashi K, Nagao M, Esumi H, Sugimura T. Food-derived mutagens and carcinogens. *Cancer Res* 1992; **52**: 2092s–8s.
2 Layton DW, Bogen KT, Knize MG, Hatch FT, Johnson VM, Felton JS. Cancer risk of heterocyclic amines in cooked foods: an analysis and implications for research. *Carcinogenesis* 1995; **16**: 39–52.
3 Nagao M, Ushijima T, Toyota M, Inoue R, Sugimura T. Genetic changes induced by heterocyclic amines. *Mutat Res* 1997; **376**: 161–7.
4 Kato T, Ohgaki H, Hasegawa H, Sato S, Takayama S, Sugimura T. Carcinogenicity in rats of a mutagenic compound, 2-amino-3,8-dimethylimidazo[4,5-f]quinoxaline. *Carcinogenesis* 1988; **9**: 71–3.
5 Ohgaki H, Hasegawa H, Suenaga M, Sato S, Takayama S, Sugimura T. Carcinogenicity in mice of a mutagenic compound, 2-amino-3,8-dimethylimidazo[4,5-f]quinoxaline (MeIQx) from cooked foods. *Carcinogenesis* 1987; **8**: 665–8.
6 Ito N, Hasegawa R, Sano M *et al.* A new colon and mammary carcinogen in cooked food, 2-amino-1-methyl-6-phenylimidazo[4,5-b]pyridine (PhIP). *Carcinogenesis* 1991; **12**: 1503–6.
7 Esumi H, Ohgaki H, Kohzen E, Takayama S, Sugimura T. Induction of lymphoma in CDF1 mice by the food mutagen, 2-amino-1-methyl-6-phenylimidazo[4,5-b]pyridine. *Jpn J Cancer Res* 1989; **80**: 1176–8.
8 Ohgaki H, Hasegawa H, Kato T *et al.* Carcinogenicity in mice and rats of heterocyclic amines in cooked foods. *Environ Health Perspect* 1986; **67**: 129–34.
9 Ohgaki H, Kusama K, Matsukura N *et al.* Carcinogenicity in mice of a mutagenic compound, 2-amino-3-methylimidazo[4,5-f]quinoline, from broiled sardine, cooked beef and beef extract. *Carcinogenesis* 1984; **5**: 921–4.
10 Adamson RH, Thorgeirsson UP, Snyderwine EG *et al.* Carcinogenicity of 2-amino-3-methylimidazo[4,5-f]quinoline in nonhuman primates: induction of tumors in three macaques. *Jpn J Cancer Res* 1990; **81**: 10–4.
11 WHO, IARC. *IARC Monographs on the Evaluation of Carcinogenic Risks to Humans: Some Naturally Occurring Substances: Food Items and Constituents, Heterocylic Aromatic Amines and Mycotoxins*. Lyon: World Health Organization, International Agency for Research on Cancer, 1993; 165–242.
12 Sofuni T, Hayashi M, Nohmi T, Matsuoka A, Yamada M, Kamata E. Semi-quantitative evaluation of genotoxic activity of chemical substances and evidence for a biological threshold of genotoxic activity. *Mutat Res* 2000; **464**: 97–104.
13 De Flora S. Detoxification of genotoxic compounds as a threshold mechanism limiting their carcinogenicity. *Toxicol Pathol* 1984; **12**: 337–43.
14 Kirkland DJ, Muller L. Interpretation of the biological relevance of genotoxicity test results: the importance of thresholds. *Mutat Res* 2000; **464**: 137–47.
15 Lutz WK, Kopp-Schneider A. Threshold dose response for tumor induction by genotoxic carcinogens modeled via cell-cycle delay. *Toxicol Sci* 1999; **49**: 110–5.
16 Parry JM. Reflections on the implications of thresholds of mutagenic activity for the labelling of chemicals by the European Union. *Mutat Res* 2000; **464**: 155–8.
17 Hoshi M, Morimura K, Wanibuchi H *et al.* No-observed effect levels for carcinogenicity and for in vivo mutagenicity of a genotoxic carcinogen. *Toxicol Sci* 2004; **81**: 273–9.
18 Fukushima S, Wanibuchi H, Morimura K *et al.* Lack of a dose-response relationship for carcinogenicity in the rat liver with low doses of 2-amino-3,8-dimethylimidazo[4,5-f]quinoxaline or N-nitrosodiethylamine. *Jpn J Cancer Res* 2002; **93**: 1076–82.

19 Bolt HM, Degen GH. Human carcinogenic risk evaluation, part II: contributions of the EUROTOX specialty section for carcinogenesis. *Toxicol Sci* 2004; **81**: 3–6.
20 Fukushima S, Wanibuchi H, Morimura K *et al.* Lack of initiation activity in rat liver of low doses of 2-amino-3,8-dimethylimidazo[4,5-f]quinoxaline. *Cancer Lett* 2003; **191**: 35–40.
21 Kushida M, Wanibuchi H, Morimura K *et al.* Dose-dependence of promotion of 2-amino-3,8-dimethylimidazo[4,5-f]quinoxaline-induced rat hepatocarcinogenesis by ethanol: evidence for a threshold. *Cancer Sci* 2005; **96**: 747–57.
22 Wei M, Hori TA, Ichihara T *et al.* Existence of no-observed effect levels for 2-amino-3,8-dimethylimidazo[4,5-f]quinoxaline on hepatic preneoplastic lesion development in BN rats. *Cancer Lett* 2006; **231**: 304–8.
23 Doi K, Wanibuchi H, Salim EI *et al.* Lack of large intestinal carcinogenicity of 2-amino-1-methyl-6-phenylimidazo[4,5-b]pyridine at low doses in rats initiated with azoxymethane. *Int J Cancer* 2005; **115**: 870–8.
24 Fukushima S, Wanibuchi H, Morimura K *et al.* Existence of a threshold for induction of aberrant crypt foci in the rat colon with low doses of 2-amino-1-methyl-6-phenolimidazo[4,5-b]pyridine. *Toxicol Sci* 2004; **80**: 109–14.
25 Ito N, Tsuda H, Tatematsu M *et al.* Enhancing effect of various hepatocarcinogens on induction of preneoplastic glutathione S-transferase placental form positive foci in rats – an approach for a new medium-term bioassay system. *Carcinogenesis* 1988; **9**: 387–94.
26 Tsuda H, Fukushima S, Wanibuchi H *et al.* Value of GST-P positive preneoplastic hepatic foci in dose-response studies of hepatocarcinogenesis: evidence for practical thresholds with both genotoxic and nongenotoxic carcinogens. A review of recent work. *Toxicol Pathol* 2003; **31**: 80–6.
27 Bird RP. Observation and quantification of aberrant crypts in the murine colon treated with a colon carcinogen: preliminary findings. *Cancer Lett* 1987; **37**: 147–51.
28 Tudek B, Bird RP, Bruce WR. Foci of aberrant crypts in the colons of mice and rats exposed to carcinogens associated with foods. *Cancer Res* 1989; **49**: 1236–40.
29 Ochiai M, Nakagama H, Turesky RJ, Sugimura T, Nagao M. A new modification of the 32P-post-labeling method to recover IQ-DNA adducts as mononucleotides. *Mutagenesis* 1999; **14**: 239–42.
30 Totsuka Y, Fukutome K, Takahashi M *et al.* Presence of N2-(deoxyguanosin-8-yl)-2-amino-3,8-dimethylimidazo[4,5-f]quinoxaline (dG-C8-MeIQx) in human tissues. *Carcinogenesis* 1996; **17**: 1029–34.
31 Wei M, Hamoud AS, Yamaguchi T *et al.* Potassium bromate enhances N-ethyl-N-hydroxyethylnitrosamine-induced kidney carcinogenesis only at high doses in Wistar rats: indication of the existence of an enhancement threshold. *Toxicol Pathol* 2009; **37**: 983–91.
32 Pretlow TP, O'Riordan MA, Somich GA, Amini SB, Pretlow TG. Aberrant crypts correlate with tumor incidence in F344 rats treated with azoxymethane and phytate. *Carcinogenesis* 1992; **13**: 1509–12.
33 Kirsch-Volders M, Vanhauwaert A, Eichenlaub-Ritter U, Decordier I. Indirect mechanisms of genotoxicity. *Toxicol Lett* 2003; **140–141**: 63–74.
34 Norbury CJ, Hickson ID. Cellular responses to DNA damage. *Annu Rev Pharmacol Toxicol* 2001; **41**: 367–401.
35 Bennett RA, Wilson DM III, Wong D, Demple B. Interaction of human apurinic endonuclease and DNA polymerase beta in the base excision repair pathway. *Proc Natl Acad Sci U S A* 1997; **94**: 7166–9.
36 Kolodner RD. Guarding against mutation. *Nature* 2000; **407**: 687–9.
37 Moller P, Wallin H, Vogel U *et al.* Mutagenicity of 2-amino-3-methylimidazo[4,5-f]quinoline in colon and liver of Big Blue rats: role of DNA adducts, strand breaks, DNA repair and oxidative stress. *Carcinogenesis* 2002; **23**: 1379–85.
38 Yang Q, Manicone A, Coursen JD *et al.* Identification of a functional domain in a GADD45-mediated G2/M checkpoint. *J Biol Chem* 2000; **275**: 36892–8.
39 O'Reilly MA, Staversky RJ, Watkins RH, Maniscalco WM, Keng PC. p53-independent induction of GADD45 and GADD153 in mouse lungs exposed to hyperoxia. *Am J Physiol Lung Cell Mol Physiol* 2000; **278**: L552–9.
40 Shaulian E, Karin M. Stress-induced JNK activation is independent of Gadd45 induction. *J Biol Chem* 1999; **274**: 29595–8.
41 Morimura K, Salim EI, Yamamoto S, Wanibuchi H, Fukushima S. Dose-dependent induction of aberrant crypt foci in the colons but no neoplastic lesions in the livers of heterozygous p53-deficient mice treated with low dose 2-amino-3-methylimidazo [4,5-f]quinoline. *Cancer Lett* 1999; **138**: 81–5.
42 Schut HA, Snyderwine EG. DNA adducts of heterocyclic amine food mutagens: implications for mutagenesis and carcinogenesis. *Carcinogenesis* 1999; **20**: 353–68.
43 Schut HA, Herzog CR, Cummings DA. Accumulation of DNA adducts of 2-amino-3-methylimidazo[4,5-f] quinoline (IQ) in tissues and white blood cells of the Fischer-344 rat after multiple oral dosing. *Carcinogenesis* 1994; **15**: 1467–70.
44 Snyderwine EG, Yamashita K, Adamson RH *et al.* Use of the 32P-postlabeling method to detect DNA adducts of 2-amino-3-methylimidazolo[4,5-f]quinoline (IQ) in monkeys fed IQ: identification of the N-(deoxyguanosin-8-yl)-IQ adduct. *Carcinogenesis* 1988; **9**: 1739–43.
45 Yamashita K, Adachi M, Kato S *et al.* DNA adducts formed by 2-amino-3,8-dimethylimidazo[4,5-f]quinoxaline in rat liver: dose-response on chronic administration. *Jpn J Cancer Res* 1990; **81**: 470–6.
46 Shimada T, Hayes CL, Yamazaki H *et al.* Activation of chemically diverse procarcinogens by human cytochrome P-450 1B1. *Cancer Res* 1996; **56**: 2979–84.
47 McPherson RA, Tingle MD, Ferguson LR. Contrasting effects of acute and chronic dietary exposure to 2-amino-3-methyl-imidazo[4,5-f]quinoline (IQ) on xenobiotic metabolising enzymes in the male Fischer 344 rat: implications for chemoprevention studies. *Eur J Nutr* 2001; **40**: 39–47.
48 Kato T, Hasegawa R, Nakae D *et al.* Dose-dependent induction of 8-hydroxyguanine and preneoplastic foci in rat liver by a food-derived carcinogen, 2-amino-3,8-dimethylimidazo[4,5-f]quinoxaline, at low dose levels. *Jpn J Cancer Res* 1996; **87**: 127–33.

doi: 10.1111/j.1349-7006.2010.01761.x

Genes and Environment, Vol. 33, No. 1 pp. 14–20 (2011)

Review

In Vitro and *In Vivo* Genotoxicity Induced by Fullerene (C_{60}) and Kaolin

Yukari Totsuka[1,5], Tatsuya Kato[1,2], Shu-ichi Masuda[2], Kousuke Ishino[1], Yoko Matsumoto[1,3], Sumio Goto[3], Masanobu Kawanishi[4], Takashi Yagi[4] and Keiji Wakabayashi[2]

[1]Division of Cancer Development System, National Cancer Center Research Institute, Tokyo, Japan
[2]Department of Food & Nutritional Science, Graduate School of Nutrition & Environmental Science, University of Shizuoka, Shizuoka, Japan
[3]Laboratory of Environmental Risk Evaluation, School of Life and Enviromental Science, Azabu University, Kanagawa, Japan
[4]Environmental Genetics Laboratory, Frontier Science Innovation Center, Osaka Prefecture University, Osaka, Japan

(Received December 11, 2010; Revised December 22, 2010; Accepted December 26, 2010)

Nanomaterials are being utilized for many kinds of industrial products, and the assessment of genotoxicity and safety of nanomaterials is therefore of concern. In the present study, we examined the genotoxic effects of fullerene (C_{60}) and kaolin using *in vitro* and *in vivo* genotoxicity systems. Both nanomaterials significantly induced micronuclei and enhanced frequency of sister chromatid exchange (SCE) in cultured mammalian cells. When ICR mice were intratracheally instilled with these nanomaterials, DNA damage of the lungs increased significantly that of the vehicle control. Formation of DNA adducts in the lungs of mice exposed to nanomaterials were also analyzed by stable isotope dilution LC-MS/MS. 8-Oxodeoxyguanosine and other lipid peroxide related adducts were increased by 2- to 5-fold in the nanomaterial-exposed mice. Moreover, multiple (four consecutive doses of 0.2 mg per animal per week) instillations of C_{60} or kaolin, increased *gpt* mutant frequencies in the lungs of *gpt* delta transgenic mice. As the result of mutation spectrum analysis, G:C to C:G transversions were commonly increased in the lungs of mice exposed to both nanomaterials. In addition, G:C to A:T was increased in kaolin-exposed mice. In immunohistochemical analysis, many regions of the lungs that stained positively for nitrotyrosine (NT) were observed in mice exposed to nanomaterials. From these observations, it is suggested that oxidative stress and inflammatory responses are probably involved in the genotoxicity induced by C_{60} and kaolin.

Key words: nanomaterials, genotoxicity, fullerene (C_{60}), kaolin, DNA adducts

Introduction

Recently, nanomaterials are being utilized for cosmetics and industrial products, and applications in medicine are under consideration. The assessment of genotoxicity and safety of nanomaterials is therefore of concern. One reason behind this is the asbestos crisis (1). Some nanomaterials are not only nano-sized particles, but also asbestos shape-like fibers, and the carcinogenic potential of such nanomaterials has attracted much attention over the years. Moreover, it is thought that nano-sized particles can be taken up in cells and cause intracellular damage (2,3). With this background, we here investigated induction of *in vitro* and *in vivo* genotoxicity using fullerene (C_{60}) and kaolin as examples. To clarify the mechanisms of mutations due to these nanomaterials, we analyzed the formation of DNA adducts in the lungs of mice after exposure. Here, we briefly summarize our data and also discuss mechanisms of genotoxicity induced by nanomaterials.

Size Distribution in Suspensions of Nanomaterials

The size distribution of nanomaterials used in the present study was analyzed by dynamic light scattering (DLS) as described previously (4). The most abundant sizes were at 234.1 ± 48.9 and 856.5 ± 119.2 nm for C_{60} and 357.6 ± 199.4 nm for kaolin, respectively.

In Vitro Genotoxicity Test

Micronucleus test: The micronucleus genotoxicity/clastogenicity test is widely used for assessment of environmental substances and medicinal chemicals. Here, we investigated the micronucleus inducing activity of C_{60} and kaolin using human lung carcinoma A549

[5]Correspondence to: Yukari Totsuka, Division of Cancer Development System, National Cancer Center Research Institute, 1-1 Tsukiji 5 Chome, Chuo-ku, Tokyo 104-0045, Japan. Tel: +81-3-3542-2511, Fax: +81-3-3543-9305, E-mail: ytotsuka@ncc.go.jp

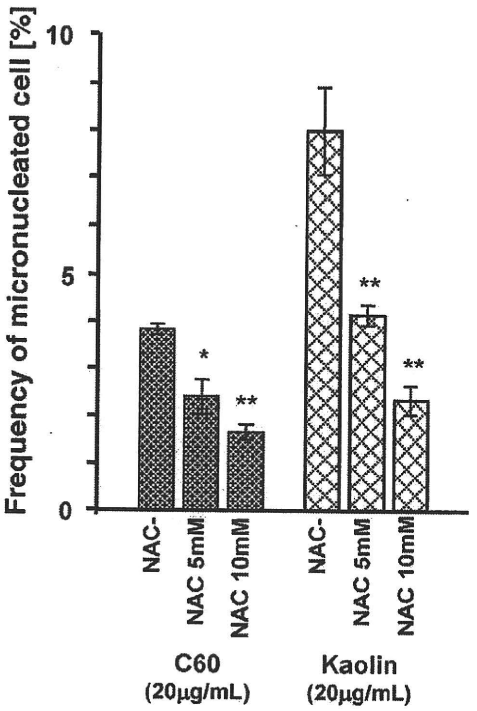

Fig. 1. Effects of anti-oxidative agents on the micronucleus inducing activity of nanoparticles. Values represent the means of three experiments ± SD. Asterisks (*, ** for $p < 0.05$ and $p < 0.01$, respectively) indicate significant differences from cells without NAC in the Student's t-test. Concentrations of nanoparticles in $\mu g/cm^2$ are given in parentheses.

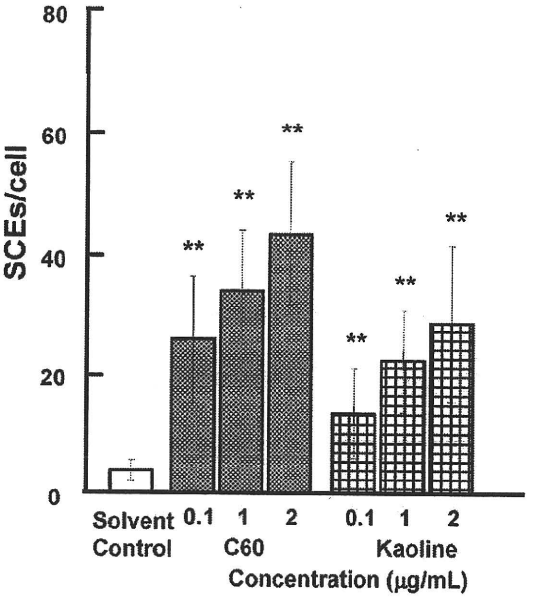

Fig. 2. Sister chromatid exchange (SCE) in CHO AA8 cells following treatment with C60 or kaolin for 1 h. The values represent the means of three experiments ± SD. Asterisks (**) indicate a significant difference ($p < 0.01$) from control (treatment with 0.005% (v/v) Tween-80) cells in the Student's t-test.

cells (4). Six-hours treatment with 200 μg/mL kaolin caused growth inhibition of 60% whereas, C_{60} at the same concentration was without effect. C_{60} and kaolin particles both increased the number of micronucleated cells. The background frequency of micronucleated cells was 0.7% to 1.0%, and this rose to 10% and 5% with 200 μg/mL of C_{60} and kaolin, respectively, the increase being statistically significant in both cases. To investigate the effects of an anti-oxidative agent on the micronucleus induction, we conducted tests with or without *N*-acetyl cysteine (NAC) using Chinese hamster ovary CHO-AA8 cells. As shown in Fig. 1, the frequency of micronucleated cells was decreased significantly in the presence of NAC. With 20 μg/mL of C_{60} and kaolin for 6 h without NAC the results were 3.8% and 8%, respectively, but in the presence of 10 mM NAC these decreased to 1.7% and 2.3%. From this observation, oxidative stress might be involved in the genotoxicity induced by nanoparticles. Furthermore, it is known that photoexcited C_{60} produces reactive oxygen species (5) and in the present experiments, the cells and C_{60} were not shielded from visible light completely. Therefore, reactive oxygen species might contribute to micronucleus-induction in C_{60}-treated cells. On the other hand, biologically relevant features of kaolin are unclear and further studies will be required to elucidate genotoxic mechanisms.

Sister chromatid exchange (SCE) test: SCE is also used for mutagenic testing of many products. While the mechanisms responsible for SCE are not completely understood, they involve breakage of both DNA strands, followed by exchange of whole DNA duplexes. This occurs during the S phase and is efficiently induced by mutagens that form DNA adducts or that interfere with DNA replication. To investigate SCE inducing activity of nanoparticles, we examined CHO-AA8 cells following 1 h treatment with C_{60} and kaolin (Fig. 2). The SCE frequencies in cells treated with 2.0 μg/mL of C_{60} and kaolin were approximately 11 and 7 times higher than the control level, respectively ($P < 0.01$ at 0.1 μg/mL or higher concentrations). C_{60} demonstrated stronger genotoxic/clastogenic potency than kaolin. Cozzi *et al.* earlier reported that H_2O_2-treatment produced reactive oxygen species and induced SCE in CHO cells, and antioxidants, such as ascorbic acid and β-carotene, reduced the frequency (6). In the present study, the results of the micronucleus test indicated involvement of reactive oxygen species so that they might contribute to SCE induction as well.

In Vivo Genotoxicity Test

Comet assay: The comet assay is known as a standard simple and sensitive technique for evaluation of

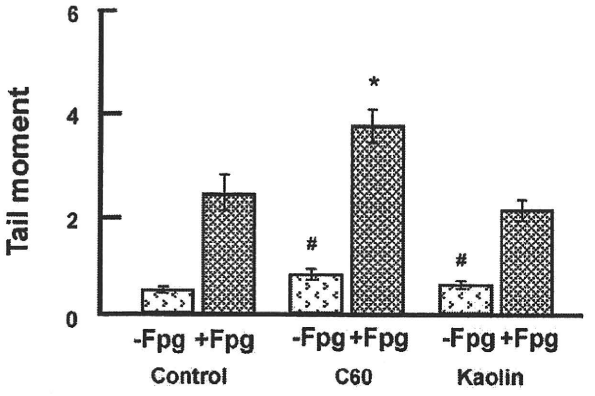

Fig. 3 DNA damage measured by comet assay in lungs of C57BL/6J mice intratracheally instilled with particles, with or without FPG treatment. Male mice were treated at a dose of 0.2 mg of particles per animal, and sacrificed 3 h after particle administration. The values represent the means of data for five animals ± SE. An asterisk (*) denotes $p < 0.01$ from that of control (+FPG) and a sharp (#) denotes $p < 0.01$ from that of control (-FPG) in a Dunnett's test after one-way ANOVA of Tail Moment.

DNA damage. The types of damage usually detected are single and double strand breaks. The pH (usually between neutral and alkaline pH) of the lysis condition can be adjusted depending upon the type of damage. Under alkaline conditions, AP sites and others where excision repair takes place are detected as DNA damage. We here evaluated DNA damage induced by particles using the comet assay under alkaline conditions. The values for DNA tail moment in the lungs with single-particle treatment at 0.2 mg/body for 3 h were measured, and DNA damage was significantly increased, around 2-fold, as compared with the vehicle control, and its intensity was C_{60} > kaolin. When we examined the effects of oxidation of purines, DNA damage was analyzed by formamidopyrimidin-glycosilase (FPG)-modified comet assay. DNA damage induced by kaolin was not changed, whereas DNA damage caused by C_{60} was elevated up to 1.7 fold compared with the vehicle control (Fig. 3). In addition, Jacobsen *et al.* also reported that C_{60} significantly increased the level of FPG sensitive sites/oxidized purines determined by the comet assay using the E1-Mutatrade markMouse lung epithelial cell line (7). From these findings, it seems that oxidative damage would be partly involved in the induction of DNA damage by C_{60}, although other changes responsible for DNA damage might be induced by kaolin.

Oxidative and lipid peroxide related DNA adduct formation: DNA adducts, formed by reactions with exogenous or endogenous agents, are known to induce gene mutations. Reactive oxygen species (ROS) are one type of endogenous agent that can produce oxidative DNA adducts such as 8-oxo-2′-deoxyguanosine (8-oxodG), a widely recognized and utilized biomarker of oxidative stress, and a major mutagenic lesion producing predominately G to T transversion mutations (8). In addition, ROS generate lipid hydroperoxides to yield heptanon-etheno (Hε)-adducts, such as HεdG, HεdA and HεdC via 4-oxo-2-nonenal (4-ONE) (9). These adducts can lead to mutations, if not repaired. We examined whether these oxidative and lipid peroxide related DNA adducts were induced in the lungs of mice by intratracheally instilled nanomaterials. 8-OxodG and three kinds of Hε-adducts were analyzed in the lungs of ICR mice 3, 24, 72 and 168 h after intratracheal instillation of 0.2 mg/body of C_{60} or kaolin, and quantified by the stable isotope dilution LC-MS/MS method described by Chou *et al.* (10). Compared with a vehicle control, DNA adduct levels were increased by about 2- to 5-fold in the lungs of mice 24 h after injection of nanoparticles (Fig. 4). The increases were time dependent until 72 h then gradually decreased within 168 h of injection (data not shown). Related to this, oxidative DNA damage was induced by intratracheal instillation of C_{60} or kaolin in the comet assay with FPG treatment, as described above. In addition, Folkmann *et al.* reported that oral gavage of C_{60} increased the levels of 8-oxodG in the liver and the lungs of F344 rats (11). Moreover, Tsurudome *et al.* described increased 8-oxodG levels induced by intratracheally instilled diesel exhaust particles in the lungs of F344 rats, and 8-oxoguanine DNA glycosylase 1 (OGG1) mRNA was also overexpressed (12). The decreased DNA adducts in the present study at 168 h may have been a result of a repair enzyme such as OGG1. This is the first observation that Hε-lipid peroxide related DNA adducts are increased by nanoparticles. Such adducts could clearly contribute to nanomaterial-induced DNA damage and mutation. Our findings suggest involvement of ROS generation, although differences between C_{60} and kaolin still require clarification.

***gpt* Mutations in the lungs of *gpt* transgenic mice:** Transgenic *gpt* delta mice are a useful model system for detecting both point mutations and large deletions (< 10 kb) (13). λEG10 transgenes carrying gpt (detection of point mutations) and *red*, *gam* (detection of deletion) genes have been integrated into mouse chromosome 17, and point mutations and deletions observed in any tissues can be detected as 6-thioguanine (6-TG) resistant colonies and Spi^- plaques, respectively. To examine *in vivo* mutagenicity of nanoparticles, *gpt* delta transgenic mice were exposed to C_{60} and kaolin at four different doses by intratracheal instillation, and *gpt* mutations were analyzed. The background *gpt* mutant frequency (MF) in lungs was $10.3 \pm 0.53 \times 10^{-6}$. MFs were significantly increased by 2 to 3-fold to $30.75 \pm 3.32 \times 10^{-6}$ ($p = 0.019$) for C_{60} and $19.30 \pm 4.82 \times 10^{-6}$ ($p \fallingdotseq 0.002$) for kaolin (4).

Moreover, we examined the mutational characteris-

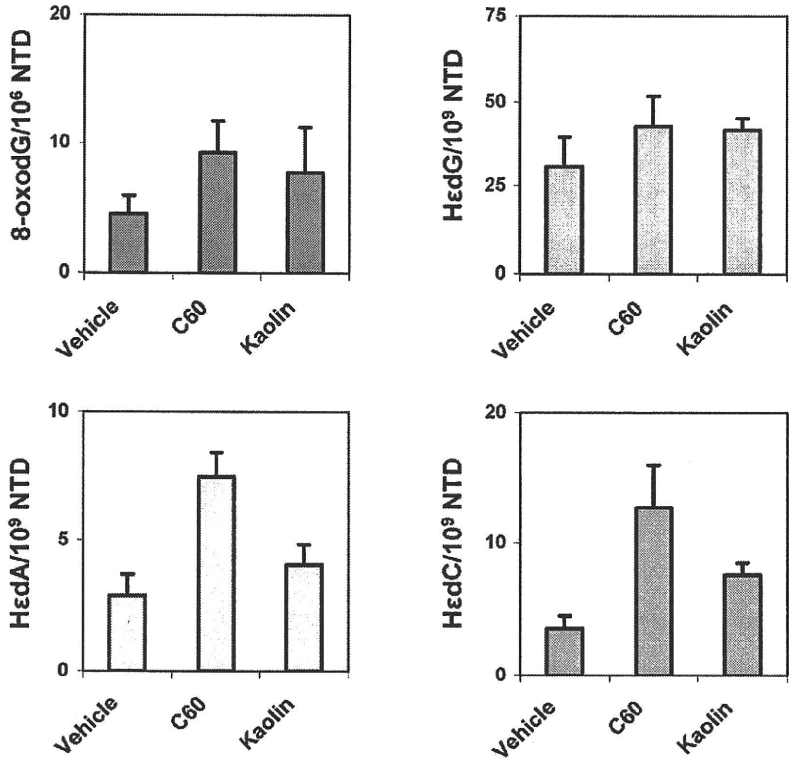

Fig. 4. Oxidative and lipid peroxide related DNA adduct formation in the lungs of ICR mice induced by nanoparticle exposure. DNA was extracted from lungs of mice 24 h after intratracheal instillation of 0.2 mg/body of C60 or kaolin, and digested enzymatically. Control animals were exposed to saline containing 0.05% Tween80. The 8-oxodG and 3 kinds of Hε-adducts were quantified by the stable isotope dilution LC-MS/MS method described by Chou *et al.* (10).

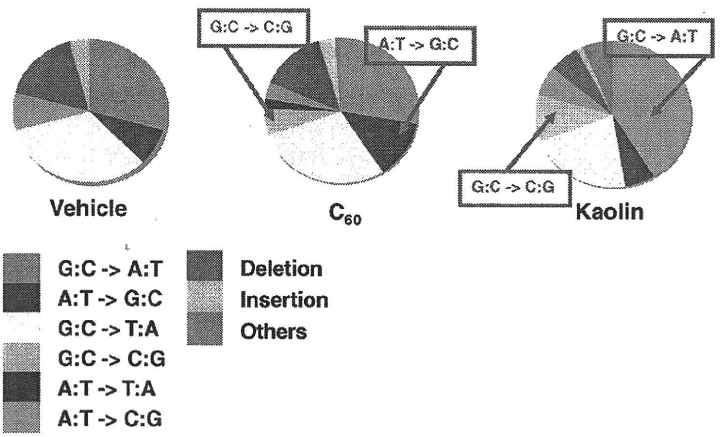

Fig. 5. Classification of *gpt* mutations from the lungs of control and nanoparticle treated mice.

tics induced by particles by PCR and DNA sequencing analysis of 6-TG resistant mutants. Classes of mutations found in the *gpt* gene are shown in Fig. 5. Interestingly, G:C to C:G transversions were increased in common with both particle treatments. Since these mutations were commonly increased regardless of the constituents (i.e., C_{60} is graphite and kaolin is aluminum silicate), the mechanisms might be the same. It has been reported that various oxidative stresses caused by sunlight, UV radiation, hydrogen peroxide and peroxy radicals frequently induce G:C to C:G transversions in various *in vitro* assay systems (14–17). Moreover, a variety of ox-

idative lesion products of guanine other than 8-oxodG, including imidazolone (Iz), oxazolone (Oz), spiroiminodihydantoin (Sp) and guanidinohydantoin (Gh), have been reported (18-24). Three such molecules, Oz, Sp and Gh are now thought to be key causes G to C transversions with translesion synthesis systems (22-25). Therefore, it is suggested that G:C to C:G transversions induced by C_{60} and kaolin could involve Oz, Sp and Gh formation. In addition, G:C to A:T transitions were also significantly increased by instillation of kaolin but not C_{60}. In general, G to A (or C to T) transitions have commonly been observed in spontaneous and chemically-induced mutants, and deamination of guanine or 5-methylcytosine might be involved. Burney *et al.* reported that nitric oxide induces DNA damage. NO· can form N_2O_3, and direct by this agent can lead to DNA deamination via diazonium ion formation (26). Moreover, nitric oxide is produced by activated macrophages in inflamed organs. In fact, test substance-phagocytized macrophages and granulomas were frequently observed in the lungs of mice (4).

Immunohistochemical Analysis of Inflammation Factors

In order to confirm enhancement of nitric oxide production by C_{60} and kaolin, we examined immunohistochemical staining of an inflammation factor, nitrotyrosine (NT), in the lungs of *gpt* delta mice treated with these nanoparticles using the same procedure reported previously (27) with minor modification. As shown in Fig. 6, the pattern of NT staining corresponded to the areas of inflammation within lung parenchyma. In the case of C_{60} exposure, many regions of the lungs stained positively (data not shown), and intense NT staining was localized in test substance-phagocytized macrophages and granulomas. Similarly, staining with NT antibodies was observed in macrophages and alveolar epithelial cells in the lungs of mice exposed to kaolin, although to a lesser extent as compared with C_{60}.

Conclusion

Our results clearly demonstrated that both *in vitro* and *in vivo* genotoxicity are induced by C_{60} and kaolin. However, the mechanisms have yet to be fully clarified, and oxidative stress might be at least partly involved. There are a number of ways in which reactive oxygen species (ROS) could be generated: i) nanoparticles might trigger ROS production by iron-catalysed Fenton reactions; ii) nanoparticles could accumulate in cells due to phagocytosis, then enhance the production of ROS by NADPH oxidase (28,29). Recently, innate immune activation through Nalp3 inflammasomes has been suggested to play an important role in pulmonary fibrotic disorders of silicosis and asbestosis (30,31). It has been reported that proinflammatory cytokines, such as interleukin 1β are key molecules for pneumoconiosis. At

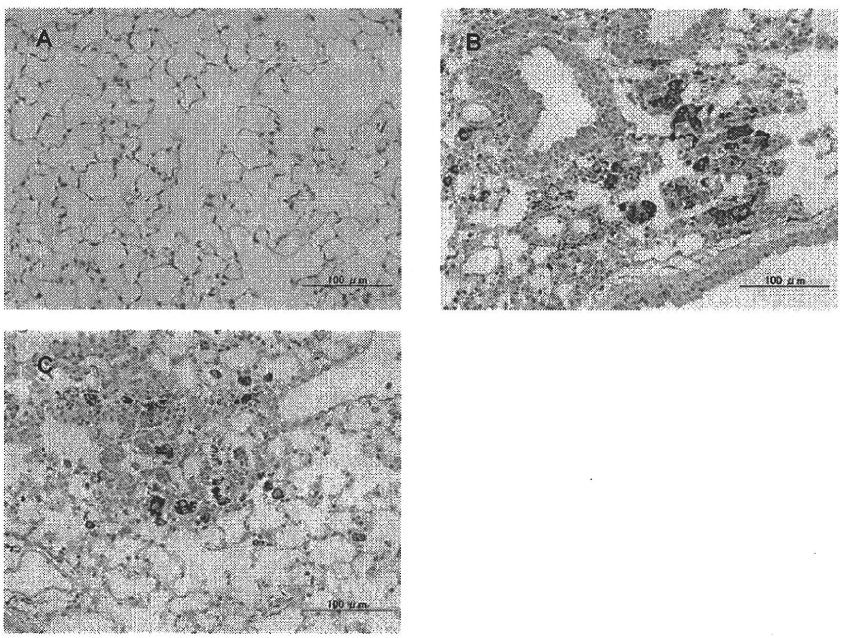

Fig. 6. Immunohistochemical localization of nitrotyrosine (NT). Since C_{60} is brown in color, we used an SG substrate kit (Vector Laboratories, USA) for peroxidase, with positive cells stained dark blue-gray. A: alveolar region in a control mouse, with no significant staining for NT. B: alveolar region in a mouse exposed to C_{60}, with positive macrophages phagocytizing test substance and epithelial cells. The brown colored material is C_{60}. C: alveolar region in a mouse exposed to kaolin. Note intense staining for NT in the granulomatous region.

present, no data are available for activation of the Nalp3 inflammasome pathway by C_{60} and kaolin. However, it is likely that both nanoparticles can activate in the same way as asbestos and silica, because oxidative stress was increased in the lungs of treated mice. Further studies of the mechanisms of genotoxicity are needed.

Acknowledgment: We thank Mr. Naoaki Uchiya and Ms Hiroko Suzuki for excellent technical assistance. This study was supported by Grants-in-Aid for Cancer Research, for the Third-Term Comprehensive 10-Year Strategy for Cancer Control, the U.S.-Japan Cooperative Medical Science Program and for Research on Risk of Chemical Substances from the Ministry of Health, Labour, and Welfare of Japan. Kousuke Ishino is presently the recipient of a Research Resident Fellowship from the Foundation for Promotion of Cancer Research.

References

1 LaDou J, Castleman B, Frank A, Gochfeld M, Greenberg M, Huff J, Joshi TK, Landrigan PJ, Lemen R, Myers J, Soffritti M, Soskolne CL, Takahashi K, Teitelbaum D, Terracini B, Watterson A. The case for a global ban on asbestos. Environ Health Perspect. 2010; 118: 897–901.

2 Nishimori H, Kondoh M, Isoda K, Tsunoda S, Tsutsumi Y, Yagi K. Histological analysis of 70-nm silica particle-induced chronic toxicity in mice. Eur J Pharm Biopharm. 2009; 72: 626–9.

3 Nabeshi H, Yoshikawa T, Matsuyama K, Nakazato Y, Arimori A, Isobe M, Tochigi S, Kondoh S, Hirai T, Akase T, Yamashita T, Yamashita K, Yoshida T, Nagano K, Abe Y, Yoshioka Y, Kamada H, Imazawa T, Itoh N, Tsunoda S, Tsutsumi Y. Size-dependent cytotoxic effects of amorphous silica nanoparticles on Langerhans cells. Pharmazie. 2010; 65:199–201.

4 Totsuka Y, Higuchi T, Imai T, Nishikawa A, Nohmi T, Kato T, Masuda S, Kinae N, Hiyoshi K, Ogo S, Kawanishi M, Yagi T, Ichinose T, Fukumori N, Watanabe M, Sugimura T, Wakabayashi K. Genotoxicity of nano/microparticles in in vitro micronuclei, in vivo comet and mutation assay systems. Part Fibre Toxicol. 2009; 6: 23.

5 Markovic Z, Trajkovic V. Biomedical potential of the reactive oxygen species generation and quenching by fullerenes (C60). Biomaterials. 2008; 29: 3561–73.

6 Cozzi R, Ricordy R, Aglitti T, Gatta V, Perticone P, De Salvia R. Ascorbic acid and beta-carotene as modulators of oxidative damage. Carcinogenesis. 1997; 18: 223–8.

7 Jacobsen NR, Pojana G, White P, Møller P, Cohn CA, Korsholm KS, Vogel U, Marcomini A, Loft S, Wallin H. Genotoxicity, cytotoxicity, and reactive oxygen species induced by single-walled carbon nanotubes and C(60) fullerenes in the FE1-Mutatrade markMouse lung epithelial cells. Environ Mol Mutagen. 2008; 49: 476–87.

8 Shi Y, Zhang JH, Jiang M, Zhu LH, Tan HQ, Lu B, Synergistic genotoxicity caused by low concentrations of titanium dioxide nanoparticles and p,p′-DDT in human hepatocytes. Environ Mol Mutagen. 2010; 51: 192–204.

9 Blair I, DNA adducts with lipid peroxidation products, J. Biol. Chem., 2008; 283: 1545–9.

10 Chou PH, Kageyama S, Matsuda S, Kanemoto K, Sasada Y, Oka M, Shinmura K, Mori H, Kawai K, Kasai H, Sugimura H, Matsuda T. Detection of lipid peroxidation-induced DNA adducts caused by 4-oxo-2(E)-nonenal and 4-oxo-2(E)-hexenal in human autopsy tissues. Chem Res Toxicol. 2010; 23:1442–8.

11 Folkmann JK, Risom L, Jacobsen NR, Wallin H, Loft S, Møller P, Oxidatively damaged DNA in rats exposed by oral gavage to C60 fullerenes and single-walled carbon nanotubes. Environ Health Perspect. 2009; 117: 703–8.

12 Tsurudome Y, Hirano T, Yamato H, Tanaka I, Sagai M, Hirano H, Nagata N, H Itoh H, Kasai H, Changes in levels of 8-hydroxyguanine in DNA, its repair and OGG1 mRNA in rat lungs after intratracheal administration of diesel exhaust particles. Carcinogenesis. 1999; 20: 1573–6.

13 Nohmi T, Masumura K. Molecular nature of intrachromosomal deletions and base substitutions induced by environmental mutagens. Environ Mol Mutagen. 2005; 45: 150–61.

14 Negishi K, Hao W. Spectrum of mutations in single-stranded DNA phage M13mp2 exposed to sunlight: predominance of G-to-C transversions. Carcinogenesis. 1992; 9: 1615–8.

15 Akasaka S, Yamamoto K. Hydrogen peroxide induces G:C to T:A and G:C to C:G transversions in the supF gene of Escherichia coli. Mol Gen Genet. 1994; 243: 500–5.

16 Valentine MR, Rodriguez H, Termini J. Mutagenesis by peroxy radicals is dominated by transversions at deoxyguanosine: evidence for the lack of involvement of 8-oxo-dG1 and/or abasic site formation. Biochemistry. 1998; 37: 7030–8.

17 Shin CY, Ponomareva ON, Connolly L, Turker MS. A mouse kidney cell line with a G:C→C:G transversion mutator phenotype. Mutat Res. 2002; 503: 69–76.

18 Kornyushyna O, Berges AM, Muller JG, Burrows CJ. In vitro nucleotide misinsertion opposite the oxidized guanosine lesions spiroiminodihydantoin and guanidinohydantoin and DNA synthesis past the lesions using Escherichia coli DNA polymerase I (Klenow fragment). Biochemistry. 2002; 41: 15304–14.

19 Cadet J, Berger M, Buchko GW, Joshi PC, Raoul S, Ravanat JL. 2,2-Diamino-4-[(3,5-di-O-acetyl-2-deoxy-.beta.-D-erythro-pentofuranosyl)amino]-5-(2H)-oxazolone: a novel and predominant radical oxidation product of 3′,5′-di-O-acetyl-2′-deoxyguanosine. J Am Chem Soc. 1994; 116: 7403–4.

20 Goyal RN, Jain N, Garg DK. Electrochemical and enzymic oxidation of guanosine and 8-hydroxyguanosine and the effects of oxidation products in mice. Bioelectrochem Bioenergetics. 1997; 43: 105–14.

21 Ye Y, Muller JG, Luo W, Mayne CL, Shallop AJ, Jones RA, Burrows CJ. Formation of 13C-, 15N-, and 18O-labeled guanidinohydantoin from guanosine oxidation with

singlet oxygen. Implications for structure and mechanism. J Am Chem Soc. 2003; 125: 13926-7.
22 Burrows CJ, Muller JG, Kornyushyna O, Luo W, Duarte V, Leipold MD, David SS. Structure and potential mutagenicity of new hydantoin products from guanosine and 8-oxo-7,8-dihydroguanine oxidation by transition metals. Environ Health Perspect. 2002; 110 Suppl 5: 713-7.
23 Kino K, Sugiyama H. UVR-induced G-C to C-G transversions from oxidative DNA damage. Mutat Res. 2005; 571: 33-42.
24 Kino K, Sugiyama H. Possible cause of G-C→C-G transversion mutation by guanine oxidation product, imidazolone. Chem Biol. 2001; 8: 369-78.
25 Kino K, Ito N, Sugasawa K, Sugiyama H, Hanaoka F. Translesion synthesis by human DNA polymerase eta across oxidative products of guanine. Nucleic Acids Symp Ser. 2004; 48: 171-2.
26 Burney S, Caulfield JL, Niles JC, Wishnok JS, Tannenbaum SR. The chemistry of DNA damage from nitric oxide and peroxynitrite. Mutat Res. 1999; 424: 37-49.
27 Porter DW, Millecchia L, Robinson VA, Hubbs A, Willard P, Pack D, Ramsey D, McLaurin J, Khan A, Landsittel D, Teass A, Castranova V. Enhanced nitric oxide and reactive oxygen species production and damage after inhalation of silica. Am J Physiol Lung Cell Mol Physiol. 2002; 283: L485-93.
28 Aust A. The role of iron in asbestos induced cancer. In: Davis JMG, Jaurand M-C, editors. Cellular and molecular effects of mineral and synthetic dusts and fibers. NATO ASI Series, Vol. H85. Berlin: Springer-Verlag; 1994. p. 53-61.
29 Mossman BT, Gee BL. Pulmonary reactions and mechanisms of toxicity of inhaled fibers. In: Gardner DE, Crapo JD, McClellan RO, editors. Toxicology of the lung. 2nd ed. New York: Raven Press; 1993. p. 371-87.
30 Dostert C, Pétrilli V, Van Bruggen R, Steele C, Mossman BT, Tschopp J. Innate immune activation through Nalp3 inflammasome sensing of asbestos and silica. Science. 2008; 320: 674-7.
31 Cassel SL, Eisenbarth SC, Iyer SS, Sadler JJ, Colegio OR, Tephly LA, Carter AB, Rothman PB, Flavell RA, Sutterwala FS. The Nalp3 inflammasome is essential for the development of silicosis. Proc Natl Acad Sci U S A. 2008; 105: 9035-40.

Cancer
Science & Therapy

Kurioka et al. J Cancer Sci Ther 2011, 3:3
http://dx.doi.org/10.4172/1948-5956.1000059

Review Article Open Access

Multicellular Spheroid Culture Models: Applications in Prostate Cancer Research and Therapeutics

Daisuke Kurioka[1], Akimitsu Takagi[2], Misao Yoneda[3], Yoshifumi Hirokawa[3], Taizo Shiraishi[3] and Masatoshi Watanabe[1]*

[1]*Laboratory for Medical Engineering, Division of Materials Science and Chemical Engineering, Graduate School of Engineering, Yokohama National University, Yokohama, Japan*
[2]*Yakult Central Institute for Microbiological Research, Tokyo, Japan*
[3]*Department of Pathologic Oncology, Institute of Molecular and Experimental Medicine, Mie University Graduate School of Medicine, Tsu, Japan*

Abstract

Prostate cancer is one of the most prevalent cancers in men in Western countries, increasing in frequency with age through the most advanced years. Patients with localized prostate cancer are generally treated with radical prostectomy or radiation therapy. However, treatment of more malignant stages of the disease is problematic. Docetaxel-based chemotherapy in men with androgen-independent prostate cancer has been shown to have survival benefits but hormonal manipulation and other chemotherapeutic regimens, especially for androgen-independent lesions, have uncertain value. While research into the complex pathophysiology of advanced prostate cancer has led to identification of mechanisms and target molecules, it nevertheless remains necessary to develop new anticancer drugs. Cell culture models that mimic the structure and features of prostate cancer *in vivo* are necessary for research on tumor biology and design of novel anticancer therapies. In this context, 3-dimensional cultures of prostate cancer cells, including multicellular spheroid (MCS) cultures, started attracting increasing attention.

The present review provides up-to-date information regarding the significance of MCS culture for identification of mechanisms underlying human malignancies, including prostate cancer, and possible targets for prostate cancer therapies.

Keywords: Multicellular spheroid (MCS); Prostate cancer; Drug resistance; Epigenetics; Poly (ADP-ribose) polymerase 1 (PARP-1)

Introduction

Prostate cancer is the most common cancer in men from Western countries, and in particular from the United States of America [1]. Incidences and mortality rates of prostate cancer vary greatly among different geographic areas and ethnic groups. In Japan, the incidence is still low compared with Western countries. However, figures are increasing [2]. Thus, Prostate cancer is the most common cancer in men in Western countries , this place having been occupied by stomach cancer in 1995 [3]. Most patients present with clinically localized disease at the time of diagnosis, and prostate-specific antigen (PSA) and transrectal ultrasound are used to aid in biopsy. Several management options are available when prostate cancer is diagnosed at an early stage, including surgery, cryosurgery, radiation therapy, hormonal therapy, and watchful waiting. For advanced prostate cancers, surgical or medical ablation of androgens is regarded as the optimal first-line treatment [4]. In most patients treated with androgen deprivation, however, disease progression will occur and result in a stage referred to as hormone-refractory prostate cancer. Development of such hormone-refractory state involves a complex series of events such as selection and outgrowth of preexisting clones of androgen-independent cells, adaptive up-regulation of genes that contribute to cancer cell survival and growth after androgen ablation [5]. However, this process is not yet entirely understood.

Patients with hormone-refractory prostate cancer (HRPC) require new agents. Two trials with docetaxel-based chemotherapy demonstrated a significant improvement in overall survival, disease-free survival, pain control, and PSA response [6,7]. Therefore, the United States Food and Drug Administration (FDA) has recommended 3-weekly docetaxel with prednisone as the first-line regimen for patients with HRPC. Despite the benefits, survival remains short and most patients actually do not benefit from docetaxel-based chemotherapy. Effective second- and third-line treatments are still urgently needed and emerging new drugs clearly require evaluation. Although the effects of several anticancer drugs for prostate cancer have been evaluated *in vitro* and in animal experiments, most have had little or no impact on the survival of patients with HRPC and metastatic prostate cancer [8]. One of the reasons for discrepancies between *in vivo* and *in vitro* experiments is thought to be the disordered arrangement of cells within the tumor tissue, in clear contrast to the ordered arrangement in 2-dimensional (2D) cultures [9,10]. Thus, preclinical experimental models mimicking the clinical characteristics of prostate cancer are a high priority for testing new agents against prostate cancer. This review covers up-to-date information regarding the significance of 3-dimensional (3D) culture models, especially multicellular spheroid (MCS) culture models for identification of mechanisms in prostate cancer and target molecules for therapy.

Three-dimensional culture models to study tumor biology

The mechanism of drug resistance is associated with overexpression of P-glycoprotein (P-gp), a protein efflux pump. Multicellular resistance (MCR), which emerges as soon as cells have established contact with their microenvironment, is also involved [11]. The development of

***Corresponding author:** Masatoshi Watanabe, M.D., Ph.D. Laboratory for Medical Engineering, Division of Materials Science and Chemical, Engineering, Graduate School of Engineering, Yokohama National University, 79-5 Tokiwadai, Hodogayaku, Yokohama, Japan; E-mail: mawata@ynu.ac.jp

Received November 06, 2010; **Accepted** January 26, 2011; **Published** February 04, 2011

Citation: Kurioka D, Takagi A, Yoneda M, Hirokawa Y, Shiraishi T, et al. (2011) Multicellular Spheroid Culture Models: Applications in prostate Cancer Research and Therapeutics. J Cancer Sci Ther 3: 060-065. doi:10.4172/1948-5956.1000059

methods to clarify the mechanisms of tumor microenvironment–mediated drug resistance is clearly important. Two-dimensional culture models have been used widely as *in vitro* models for drug discovery in the field of cancer biology. They are easy and convenient to set up but lack tumor tissue features like tumor cell–tumor cell, tumor cell–stromal cell, and tumor cell–extracellular matrix (ECM) interactions as well as its typical structural architecture. Cancer cells are also labile, and their behavior can be modulated by the extracellular microenvironment and culture conditions. Comparison between the gene expression patterns of tumor tissues and immortalized cell lines has highlighted some transcriptional modifications in response to the *in vitro* environment [12-14]. Proteome analysis of 3D compared with 2D colon cancer cell cultures revealed a panel of alterations that may affect a wide variety of cellular functions related to protein synthesis, proliferation, regulation of the cytoskeleton, and apoptosis [15]. In 2D culture models, genes associated with cell cycling, metabolism, and turnover of macromolecules are up-regulated, showing that tumor cells adapt to growth needs and respond to growth factors in the culture medium [12,16,17]. On the other hand, tumor cells repress the expression of genes that may limit their growth potential or that are not necessary for *in vitro* growth. Thus, the value of 2D culture models for cancer research is limited. Importantly, it needs to be stressed that animal test systems are indispensable for pharmacokinetic and toxicological evaluation of candidate therapeutic compounds. However, the number of animal models used in the initial discovery of lead compounds has already begun to decline because of ethical and economic concerns, as well as inaccuracy for predicting clinical efficacy. The same is expected to happen with regard to target validation [18].

Some 3D culture models may satisfy the demands comparatively well and are thus promising tools for anticancer drug screening [19]. Notably, MCS can be cocultured with immune cells to evaluate the efficacy of immunotherapy, which progresses to future-oriented culture models [20]. The 3D culture models known at present are listed in (Table 1).

MCS culture models of prostate cancer cells

MCS culture is a 3D culture technique that closely mimics the tumor microenvironment. As for the case of other malignancies, MCS culture

Model	Method	Description
Multicellular spheroid		Spherical aggregate of cells in static or stirred suspension culture
	Spontaneous aggregation Liquid-overlay	A small number of cell types forms clusters rather than strict spheroids Cells cultured on the surface of an agarose gel matrix which blocks attachment of the cells
	Microcarrier beads	Beads support aggregation of attached dependent cells to form pseudo-spheroids in gyratory and spinner flasks
	Spinner flask	Greater quantities of spheroids can be cultivated in suspension than in liquid-overlay cultures
	Gyratory shaker	Cell suspensions in Erlenmeyer flasks containing a specific amount of medium are rotated in a gyratory rotation incubator
	Rotary cell culture	The low shear environment provides an advantage over static and stirred cultures, allowing cells to aggregate, grow like 3D structure and differentiate
Cellular multilayer		Layers of cells cultured on top of a porous membrane
Scaffold-based culture		Cells cultured in synthetic 3D-simulating matrices
Hollow-fiber bioreactor		Cells cultured within a network of perfused artificial capillaries

Table 1: Summary of three-dimensional culture models [16,18].

models of prostate cancer cells have been used to study prostate tumor biology, tumor cell–stromal cell interactions, and tumor cell responses to therapy [13,21-40] Recently, a comprehensive panel of spheroid culture models, including normal epithelial cells, their derivatives, and classical prostate cancer cell lines, has been reported [41]. As for MCS culture methods, spontaneous aggregation, liquid overlay, spinner flask, and rotating-wall vessel models have been used. Liquid overlay cultures exhibit enhanced functions relative to 2D cultures [23,25,31]. We have used round-bottomed plates coated with poly (2-hydroxyethyl methacrylate) (poly-HEMA; Sigma. Inc., St. Louis, MO) to monitor and manipulate arranged single spheroids at particular growth stages. Under some culture conditions, MCS of prostate cancer cell lines appear to be induced through enhanced expression of E-cadherin. PC-3 (human prostate cancer cell line) cells exhibiting abnormal E-cadherin–mediated cell–cell adhesion are unable to form compact spheroids or tight aggregates, yet loose aggregation in a liquid overlay culture has been reported [13,23,25-31,42]. Moreover, treatment with an anti–E-cadherin antibody inhibits spheroid formation of DU-145 (human prostate carcinoma, epithelial-like cell line) and LNCaP (human prostate adenocarcinoma cell line) cells (Figure1). Besides its function in the formation of MCS, E-cadherin plays an important role in suppression of anoikis [43]. Aggregation of PC-3 cells rather than MCS formation occurs on agar- or poly-HEMA–coated plates; on Matrigel, a one-cell-thick spheroid is formed that partially induces normal differentiation of PC-3 cells [23,25,28]. These findings suggest that MCS formation may be dependent on tumor cell adhesion molecules and culture conditions. In addition, different MCS formation techniques may lead to different MCS phenotypes with different gene expression patterns [44]. Thus, it is essential to carefully select the most appropriate method.

DU-145 cells form fused compact spheroids, and both DU-145 and LNCaP cells grow at significantly slower rates than in 2D culture [23,25]. MCS of LNCaP cells exhibit disordered but tight cell–cell contacts, and their characteristics differ according to the location [13]. In two studies, the tumor cells of the intermediate zone were found to be positive for p27 and poly (ADP-ribose) polymerase 1 (PARP-1), but negative for Ki-67 (Figure 2a) [13,45]. These cells thus appear to be quiescent. All in all, the structure of a MCS is heterogeneous, with proliferating cells at the periphery and necrotic cells at the center [10,13]. Quiescent cells are viable but remain in a reversible state of growth arrest. The mechanism of their development within MCS remains unclear but appears to be a consequence of microenvironmental factors such as deprivation of growth factors and/or nutrients [10,13,46]. In general, slow-growing tumors tend to be more drug- or ionizing radiation–resistant than rapidly growing tumors. There is no indication as to whether the proportion of quiescent cells is higher in MCS [11]. However, the presence and proportion of quiescent cells may be important determinants of the efficacy of chemotherapy

Differential expression of p18INK4c, p21waf1/cip1, and p27kip1 with respect to their location in the spheroids of EMT6 (mouse mammary tumor cell line) and MEL28 (human melanoma cell line) cells has also been reported: p21waf1/cip1 is found in the outer, proliferating cells, whereas p18INK4c and p27kip1 expression becomes elevated with increasing depth [47]. A decrease in all cell cycle regulatory proteins such as cyclin-dependent kinases (CDKs), CDK inhibitors (CKIs), and cyclins in the innermost spheroid fraction has also been observed [47]. These findings suggest molecular regulation of cell cycle progression in the inner region of spheroids due to microenvironmental stress and hypoxia, which evokes cell cycle arrest via the cyclin-dependent kinase inhibitor p27kip1 [48]. Quiescence was found due to marked

cell contact–dependent up-regulation of p27kip1 in EMT6 spheroids, leading to drug or radiation resistance [49,50]. Ki-67 is a nuclear protein expressed during all active phases of the cell cycle. Therefore, it is expressed in proliferating but not in quiescent cells [10,13,46]. In contrast, a dramatic increase of p27kip1 was detected in every cell of the MCS in response to serum withdrawal, which is thought to be a specific environment [46]. In addition, up-regulation of P-gp in G0/G1-phase cells requires expression of p27kip1 but not of p21waf1, suggesting that, under stress conditions (for instance, in hypoxia), p27kip1 contributes to a cell cycle arrest that is essential for cell survival, whereas P-gp contributes to cell survival by helping detoxify waste products [51].

PARPs are enzymes present in eukaryotes; these enzymes are involved in cell signaling through poly (ADP-ribosyl) ation of DNA-binding proteins [52,53]. By catalyzing the addition of ADP-ribose units to DNA, histones, and various DNA repair enzymes, they play multifunctional roles in many cellular processes. PARP-1 (EC 2.4.2.30) was the first of this family to be described in association with cellular responses to DNA damage [52,53]. PARP-1 has a critical role in the repair of DNA single-strand breaks (SSB) through excision repair pathway. In addition, PARP-1 binds to DNA double-strand breaks (DSB) and activates several proteins involved in homologous recombination repair and nonhomologous end-joining pathways. Besides being involved in DNA repair, PARP can also act as a mediator of cell death [53]. Extensive DNA damage is known to trigger PARP overactivation with consequent extensive NAD consumption through ADP-ribose polymer synthesis, leading to ATP depletion and induction of necrosis.

In human malignancies, increased expression of PARP-1 has been reported in Ewing's sarcomas and in malignant lymphomas; conversely, decreased PARP-1 expression has been found in breast cancer and several other cell lines [53]. High PARP expression in prostate cancer cell lines compared to benign cell lines has already been reported, in which greater than 90% of LNCaP cells showed positivity for PARP before and after treatment with H2O2 [54]. In LNCaP spheroids, expression of PARP-1 was detected and confined to the intermediate zone (Figure 2a) [37,45], but real-time PCR demonstrated that expression of PARP-1 in 2D cultures is higher than in spheroid cultures. The specific location means that PARP maycontribute to the characteristics of the quiescent cells within the LNCaP spheroids, being linked with the target molecule in prostate cancer treatments. However, [55] reported that in glioma spheroids, PARP expression, which is initially diffuse, becomes confined to the outer proliferative zone, paralleling the expression of Ki-67. The authors speculated that this phenomenon might be consistent with a role for PARP in cell proliferation and determination of the biological behavior of gliomas.

Epigenetic mechanisms that can affect gene expression without altering the actual sequence of DNA include DNA methylation,

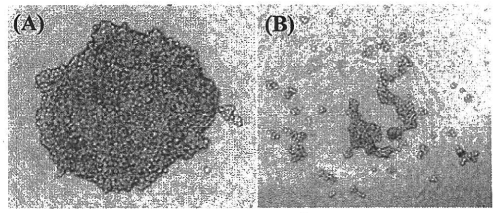

Figure 1: Role of E-cadherin in the formation of a LNCaP spheroid. (A) LNCaP cells form spheroids when cultured on poly-HEMA-coated dishes. (B) Treatment with an anti- E-cadherin antibody (HECD-1) inhibits LNCaP spheroid formation (Takagi et al., unpublished data).

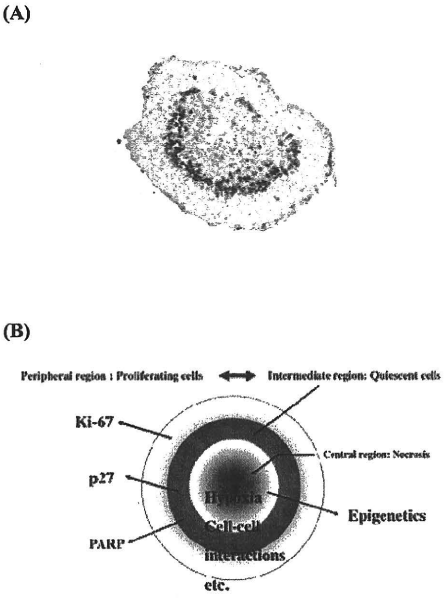

Figure 2: Localization of PARP-1 in a LNCaP spheroid and structure of a multicellular spheroid (MCS). (A) A section of a 7-day spheroid was stained with an anti-PARP-1 antibody (A6.4.12; Serotec, Oxford, UK). There is the intermediate zone with PARP immunostaining. (B) Structure of a MCS and characteristics of the tumor microenvironment. The structure of the spheroid favors genetic and epigenetic alterations.

RNA-associated silencing, and histone modification. These phenomena importantly affect gene expression during development [56]. Methylation of the C5 position of cytosine residues in DNA is recognized as a particularly important epigenetic silencing mechanism. Histone modification is another important epigenetic mechanism that determines their interactions with other proteins, thereby regulating chromatin structure and remodeling. DNA methylation and histone modifications related to chromatin remodeling have been intensively analyzed in various tumor types [57]. Thus, it is interesting to examine the epigenetic state of cancer cells in spheroids. [58] found that, similar to spheroids, TSUPr1 cells dynamically change their methylation patterns and the expression of E-cadherin as a function of the cellular microenvironment. They distinctively speculated that the cellular microenvironment selects for cells that have an appropriate methylation pattern, and that spheroid formation may increase the transcriptional expression E-cadherin, which in turn may drive regional hypomethylation of densely methylated CpG islands. This finding is very interesting because a methylation-regulated gene in a spheroid culture changes within a few days as compared to 2D cultures. A recent study by [59] has shown that increased levels of heterochromatin in spheroids characterized by histone H3 deacetylation and increased heterochromatin protein 1α expression result in improved radiation survival and reduced numbers of DNA DSBs and lethal chromosome aberrations. A previous report showed that 3D growth of mammary epithelial cells reduced histone H3 and H4 acetylation and gene expression, although ECM-controlled cell shape was discussed [60]. Few studies about DNA methylation in spheroids have been reported. Similarly, little is known about the action of DNA methyltransferase (DNMT) enzymes. However, preliminary data showed that there are no significant differences in long interspersed nucleotide element 1 (LINE-1) hypomethylation between 2D culture and MCS of LNCaP cells [37].

The microenvironment of solid tumors such as prostate cancer is characterized by hypoxia, low extracellular pH, and nutrient deprivation. Under hypoxia, tumor cells increase expression of various genes, for instance those contributing to angiogenesis, partially through hypoxia-induced factor 1 (HIF-1). On the other hand, genes involved in cellular adhesion and DNA repair are decreased [61]. Down-regulation of mutL homologue 1 (MLH-1) in 2D cultures of EMT-6 cells under hypoxic conditions has been detected, with PM2 expression being unchanged [62]. However, down-regulation of PM2 was detected in EMT-6 spheroids. These results suggest that tumors can down-regulate DNA mismatch repair as a result of a series of microenvironmental factors, which results in increased resistance to alkylating agents. It has been hypothesized that hypoxia may influence local epigenetic alterations, leading to inappropriate silencing and reawakening of cancer genes [63]. A reduction of 5-methylcytosine in xenografts compared to the levels in the same cancer cell lines *in vitro* has been reported, providing direct evidence that epigenetic events in solid tumors may be modulated by microenvironmental stress [64]. In several mammalian cell lines, hypoxia increases globaldimethylated histone H3 lysine 9 (H3K9me2) expression through histone methyltransferase G9a, leading to inhibition of gene expression [64].

These findings suggest that epigenetic alterations in spheroids may be linked to their microenvironment. Whether activation or stimulation of anticancer drug resistance–related genes such as MDR-1 is brought about by epigenetic events is an intriguing possibility that needs to be analyzed.

Applications to prostate cancer therapy

Like solid tumors in vivo, MCS is characterized by hypoxic regions, The presence of hypoxic tumor microenvironment correlates with increased tumor invasiveness, metastases, and resistance to chemotherapy and radiotherapy [65]. Chemotherapeutic drug resistance in cancer cells under hypoxia is partially caused by reduced toxicity because of the absence of molecular oxygen. Hypoxia and nutrient deprivation can also promote mitochondrial reactive oxygen species (ROS) production, which result in modulation of ROS levels and energy metabolism to activate many signalling pathways leading to HIF family protein stabilization and activation [66]. Chemotherapeutic drug resistance is caused by HIF family–induced inhibition of cell cycle progression and proliferation.

Androgen ablation leads to an initial favorable response in patients. However, most relapse with an aggressive form of the disease known as castration-resistantor hormone-refractory prostate cancer. As critical molecular events that lead to prostate cancer cell resistance to androgen-deprivation therapy have been reported, there is also a possibility that hypoxia may be involved in the transition to androgen independence. Crosstalk between the androgen receptor and HIF-1α in prostate cancer cells has been reported [67]. Thus, methods of targeting the microenvironment, especially hypoxia, have been investigated, e.g., to increase the oxygen supply to the tumor hypoxic area, to exploit the microenvironment by using bioreductive drugs, and to exploit the biological response to hypoxia by targeting HIF-1α.

PARP has attracted considerable attention as a therapeutic target for various diseases including cancer. Enhanced PARP-1 expression and/or its activity has been shown in several tumor cell lines, contributing to resistance to genotoxic stress and ability to survive exposure to DNA-damaging agents [52,53]. Inhibition of PARP-1 thus enhances the efficiency of alkylating agents and ionizing radiation [53]. These results have stimulated the development of specific PARP-1 inhibitors as potential chemoand radiosensitizers. Several small-molecule PARP inhibitors have indeed been synthesized and introduced into the clinic for treatment of cancer patients [53]. Research into breast cancer 2 susceptibility protein (BRCA2)-deficient cells, which are highly sensitive to inhibitors of PARP, has provided the basis for new therapeutic approaches [53]. Recently, a PARP inhibitor has been reported to radiosensitize DU-145 cells under hypoxia [68]. Like PARP, other proteins expressed by quiescent cells in MCSs may constitute targets for prostate cancer therapy.

The cancer stem cell (CSC) theory has emerged as a paradigm shift in our understanding of cancer as a disease of stem cells. A small subset of cancer cells within the tumor mass has the exclusive capacity to divide and expand the CSC pool and to differentiate into nontumorigenic, more differentiated cancer cell lineages. The existence of these small subsets of cells is responsible for tumor recurrence and metastasis. Thus, effective therapeutics should target rare CSCs that sustain tumor malignancy [69]. Such small subsets have been detected not only in malignancies of the blood but also in solid tumors in the brain, breast, and prostate, among others. Recent studies with prostate cells have also shown that nonmalignant immortalized cell lines and malignant cell lines contain a subset of cells with stem cell properties. In the spheroid culture system, nonmalignant and malignant human hTERT-immortalized prostate epithelial cells have been reported to maintain high CD133 expression [70]. The spheroid culture methods appear to contribute to the identification of CSCs from the prostate, which may be a new target for prostate cancer therapy.

Summary

MCS culture models have become a mainstream culture model for tumor biology and identification of anticancer resistance mechanisms as an alternative to the classical 2D culture models that poorly reflect the structural characteristicsseen in vivo. MCS culture models better mimic the growth characteristics of in vivo solid tumors. Like other solid tumors, prostate cancer creates a microenvironment characterized by hypoxia, acidosis, and nutrient deprivation, which collectively lead to tumor genetic and adaptive changes (Figure 2b). The tumor microenvironment correlates with prostate cancer invasiveness, metastasis, and resistance to radiotherapy and chemotherapy. Hypoxia may also be involved in the transition of prostate cancer to androgen independence. MCS culture models are a good model for understanding the mechanisms of resistance to chemotherapy, radiotherapy, and androgen ablation, and discovery of new targets for prostate cancer, especially androgen-independent cancer. Our review has highlighted the characteristics of prostate cancer MCS (p27 and PARP expression, and epigenetics), and underlined the tumor microenvironment as target for prostate cancer therapy. MCS culture models appear to contribute to the identification of CSCs from the prostate.

Further studies are needed to clarify mechanisms such as epigenetic regulation, to better characterize the formation of MCS, and to apply this knowledge into prostate cancer biology and the discovery of new targets for prostate cancer.

Acknowledgments

This work was supported in part by a Grant-in-Aid for Scientific Research from the Ministry of Education, Culture, Sports, Science and Technology, and a Grant-in-Aid from the Yokohama National University Global COE Program.

References

1. Jemal A, Siegel R, Ward E, Hao Y, Xu J, et al. (2008) Cancer statistics, 2008. CA Cancer J Clin 58: 71-96.

2. Watanabe M, Nakayama T, Shiraishi T, Stemmermann GN, Yatani R (2000) Comparative studies of prostate cancer in Japan versus the United States: A review. Urol Oncol 5: 274-283.

3. Tabata N, Ohno Y, Matsui R, Sugiyama H, Ito Y, et al. (2008) Partial cancer prevalence in Japan up to 2020: estimates based on incidence and survival data from population-based cancer registries. Jpn J Clin Oncol 38: 146-157.

4. Bhandari MS, Petrylak DP, Hussain M (2005) Clinical trials in metastatic prostate cancer-has there been real progress in the past decade? Eur J Cancer 41: 941-953.

5. So A, Gleave M, Hurtado-Col A, Nelson C (2005) Mechanisms of the development of androgen independence in prostate cancer. World J Urol 23: 1-9.

6. Petrylak DP, Tangen CM, Hussain MH, Lara PN Jr, Jones JA, et al. (2004) Docetaxel and estramustine compared with mitoxantrone and prednisone for advanced refractory prostate cancer. N Engl J Med 351: 1513-1520.

7. Tannock IF, de Wit R, Berry WR, Horti J, Pluzanska A, et al. (2004) Docetaxel plus prednisone or mitoxantrone plus prednisone for advanced prostate cancer. N Engl J Med 351: 1502-1512.

8. Diaz M, Patterson SG (2004) Management of androgen-independent prostate cancer. Cancer Control 11: 364-373.

9. Sutherland RM, McCredie JA, Inch WR (1971) Growth of multicell spheroids in tissue culture as a model of nodular carcinomas. J Natl Cancer Inst 46: 113-120.

10. Hirschhaeuser F, Menne H, Dittfeld C, West J, Mueller-Klieser W, et al. (2010) Multicellular tumor spheroids: an underestimated tool is catching up again. J Biotechnol 148: 3-15.

11. Desoize B, Jardillier J (2000) Multicellular resistance: a paradigm for clinical resistance? Crit Rev Oncol Hematol 36: 193-207.

12. Birgersdotter A, Sandberg R, Ernberg I (2005) Gene expression perturbation in vitro--a growing case for three-dimensional (3D) culture systems. Semin Cancer Biol 15: 405-412.

13. Takagi A, Watanabe M, Ishii Y, Morita J, Hirokawa Y, Matsuzaki T, et al. (2007) Three-dimensional cellular spheroid formation provides human prostate tumor cells with tissue-like features. Anticancer Res 27: 45-53.

14. De Witt Hamer PC, Van Tilborg AA, Eijk PP, Sminia P, Troost D, et al. (2008) The genomic profile of human malignant glioma is altered early in primary cell culture and preserved in spheroids. Oncogene 27: 2091-2096.

15. Gaedtke L, Thoenes L, Culmsee C, Mayer B, Wagner E (2007) Proteomic analysis reveals differences in protein expression in spheroid versus monolayer cultures of low-passage colon carcinoma cells. J Proteome Res 6: 4111-4118.

16. Kim JB (2005) Three-dimensional tissue culture models in cancer biology. Semin Cancer Biol 15: 365-377.

17. Rodríguez-Enríquez S, Gallardo-Pérez JC, Avilés-Salas A, Marín-Hernández A, Carreño-Fuentes L, et al. (2008) Energy metabolism transition in multi-cellular human tumor spheroids. J Cell Physiol 216: 189-197.

18. Kunz-Schughart LA, Freyer JP, Hofstaedter F, Ebner R (2004) The use of 3-D cultures for high-throughput screening: the multicellular spheroid model. J Biomol Screen 9: 273-285.

19. Burdett E, Kasper FK, Mikos AG, Ludwig JA (2010) Engineering tumors: a tissue engineering perspective in cancer biology. Tissue Eng Part B Rev 16: 351-359.

20. Gottfried E, Kunz-Schughart LA, Andreesen R, Kreutz M (2006) Brave little world: spheroids as an in vitro model to study tumor-immune-cell interactions. Cell Cycle 5: 691-695.

21. Donaldson JT, Tucker JA, Keane TE, Walther PJ, Webb KS (1990) Characterization of a new model of human prostatic cancer: the multicellular tumor spheroid. Int J Cancer 46: 238-244.

22. Ingram M, Techy GB, Saroufeem R, Yazan O, Narayan KS, et al. (1997) Three-dimensional growth patterns of various human tumor cell lines in simulated microgravity of a NASA bioreactor. In Vitro Cell Dev Biol Anim 33: 459-466.

23. Hedlund TE, Duke RC, Miller GJ (1999) Three-dimensional spheroid cultures of human prostate cancer cell lines. Prostate 41: 154-165.

24. O'Connor KC (1999) Three-dimensional cultures of prostatic cells: tissue models for the development of novel anti-cancer therapies. Pharm Res 16: 486-493.

25. Frankel A, Man S, Elliott P, Adams J, Kerbel RS (2000) Lack of multicellular drug resistance observed in human ovarian and prostate carcinoma treated with the proteasome inhibitor PS-341. Clin Cancer Res 6: 3719-3728.

26. Clejan S, O'Connor K, Rosensweig N (2001) Tri-dimensional prostate cell cultures in simulated microgravity and induced changes in lipid second messengers and signal transduction. J Cell Mol Med 5: 60-73.

27. Enmon RM Jr, O'Connor KC, Lacks DJ, Schwartz DK, Dotson RS (2001) Dynamics of spheroid self-assembly in liquid-overlay culture of DU 145 human prostate cancer cells. Biotechnol Bioeng 72: 579-591.

28. Lang SH, Stark M, Collins A, Paul AB, Stower MJ, Maitland NJ (2001) Experimental prostate epithelial morphogenesis in response to stroma and three-dimensional Matrigel culture. Cell Growth Differ 12: 631-640.

29. Enmon RM Jr, O'Connor KC, Song H, Lacks DJ, Schwartz DK (2002) Aggregation kinetics of well and poorly differentiated human prostate cancer cells. Biotechnol Bioeng 80: 580-588.

30. Mitrofanova E, Hagan C, Qi J, Seregina T, Link C Jr (2003) Sodium iodide symporter/radioactive iodine system has more efficient antitumor effect in three-dimensional spheroids. Anticancer Res 23: 2397-2404.

31. Khoei S, Goliaei B, Neshasteh-Riz A, Deizadji A (2004) The role of heat shock protein 70 in the thermoresistance of prostate cancer cell line spheroids. FEBS Lett 561: 144-148.

32. Song H, David O, Clejan S, Giordano CL, Pappas-Lebeau H, et al. (2004a) Spatial composition of prostate cancer spheroids in mixed and static cultures. Tissue Eng 10: 1266-1276.

33. Song H, Jain SK, Enmon RM, O'Connor KC (2004b) Restructuring dynamics of DU 145 and LNCaP prostate cancer spheroids. In Vitro Cell Dev Biol Anim 40: 262-267.

34. O'Connor KC, Venczel MZ (2005) Predicting aggregation kinetics of DU 145 prostate cancer cells in liquid-overlay culture. Biotechnol Lett 27: 1663-1668.

35. Wang R, Xu J, Juliette L, Castilleja A, Love J, et al. (2005) Three-dimensional co-culture models to study prostate cancer growth, progression, and metastasis to bone. Semin Cancer Biol 15: 353-64.

36. Jung V, Wullich B, Kamradt J, Stöckle M, Unteregger G (2007) An improved in vitro model to characterize invasive growing cancer cells simultaneously by function and genetic aberrations. Toxicol In Vitro 21: 183-190.

37. Watanabe M, Takagi A (2008) Biological behavior of prostate cancer cells in 3D culture systems. Yakugaku Zasshi 128: 37-44.

38. Pearson JF, Hughes S, Chambers K, Lang SH (2009) Polarized fluid movement and not cell death, creates luminal spaces in adult prostate epithelium. Cell Death Differ 16: 475-482.

39. Chu JH, Yu S, Hayward SW, Chan FL (2009) Development of a three-dimensional culture model of prostatic epithelial cells and its use for the study of epithelial-mesenchymal transition and inhibition of PI3K pathway in prostate cancer. Prostate 69: 428-442.

40. Hsiao AY, Torisawa YS, Tung YC, Sud S, Taichman RS, et al. (2009) Microfluidic system for formation of PC-3 prostate cancer co-culture spheroids. Biomaterials 30: 3020-3027.

41. Härmä V, Virtanen J, Mäkelä R, Happonen A, Mpindi JP, et al. (2010) A comprehensive panel of three-dimensional models for studies of prostate cancer growth, invasion and drug responses. PLoS One 5: e10431.

42. Mitchell S, Abel P, Ware M, Stamp G, Lalani E (2000) Phenotypic and genotypic characterization of commonly used human prostatic cell lines. BJU Int 85: 932-944.

43. Kang HG, Jenabi JM, Zhang J, Keshelava N, Shimada H, et al. (2007) E-cadherin cell-cell adhesion in ewing tumor cells mediates suppression of anoikis through activation of the ErbB4 tyrosine kinase. Cancer Res 67: 3094-3105.

44. Steadman K, Stein WD, Litman T, Yang SX, Abu-Asab M, et al. (2008) PolyHEMA spheroids are an inadequate model for the drug resistance of the intractable solid tumors. Cell Cycle 7: 818-829.

45. Muggia FM, Peters GJ, Landolph JR Jr (2009) XIII International Charles Heidelberger Symposium and 50 Years of Fluoropyrimidines in Cancer Therapy Held on September 6 to 8, 2007 at New York University Cancer Institute, Smilow Conference Center. Mol Cancer Ther 8: 992-999.

46. Mellor HR, Ferguson DJ, Callaghan R (2005) A model of quiescent tumour

microregions for evaluating multicellular resistance to chemotherapeutic drugs. Br J Cancer 93: 302-309.

47. LaRue KE, Khalil M, Freyer JP (2004) Microenvironmental regulation of proliferation in multicellular spheroids is mediated through differential expression of cyclin-dependent kinase inhibitors. Cancer Res 64: 1621-1631.
48. Gardner LB, Li Q, Park MS, Flanagan WM, Semenza GL, et al. (2001) Hypoxia inhibits G1/S transition through regulation of p27 expression. J Biol Chem 276: 7919-7926.
49. St Croix B, Florenes VA, Rak JW, Flanagan M, Bhattacharya N, et al. (1996) Impact of the cyclin-dependent kinase inhibitor p27Kip1 on resistance of tumor cells to anticancer agents. Nat Med 2: 1204-1210.
50. St Croix B, Sheehan C, Rak JW, Florenes VA, Slingerland JM, et al. (1998) E-Cadherin-dependent growth suppression is mediated by the cyclin-dependent kinase inhibitor p27(KIP1). J Cell Biol 142: 557-571.
51. Wartenberg M, Fischer K, Hescheler J, Sauer H (2002) Modulation of intrinsic P-glycoprotein expression in multicellular prostate tumor spheroids by cell cycle inhibitors. Biochim Biophys Acta 1589: 49-62.
52. Masutani M, Nozaki T, Nakamoto K, Nakagama H, Suzuki H, Kusuoka, et al. (2000) The response of Parp knockout mice against DNA damaging agents. Mutat Res 462: 159-166.
53. Ratnam K, Low JA (2007) Current development of clinical inhibitors of poly(ADP-ribose) polymerase in oncology. Clin Cancer Res 13: 1383-1388.
54. McNealy T, Frey M, Trojan L, Knoll T, Alken P, et al. (2003) Intrinsic presence of poly (ADP-ribose) is significantly increased in malignant prostate compared to benign prostate cell lines. Anticancer Res 23: 1473-1478.
55. Wharton SB, McNelis U, Bell HS, Whittle IR (2000) Expression of poly(ADP-ribose) polymerase and distribution of poly(ADP-ribosyl)ation in glioblastoma and in a glioma multicellular tumour spheroid model. Neuropathol Appl Neurobiol 26: 528-35.
56. Watanabe M, Takagi A, Matsuzaki T, Kami D, Toyota M, et al. (2006) Knowledge of epigenetic influence for prostate cancer therapy. Curr Cancer Drug Targets 6: 533-551.
57. Sharma S, Kelly TK, Jones PA (2010) Epigenetics in cancer. Carcinogenesis 31: 27-36.
58. Graff JR, Gabrielson E, Fujii H, Baylin SB, Herman JG (2000) Methylation patterns of the E-cadherin 5' CpG island are unstable and reflect the dynamic, heterogeneous loss of E-cadherin expression during metastatic progression. J Biol Chem 275: 2727-2732.
59. Storch K, Eke I, Borgmann K, Krause M, Richter C, et al. (2010) Three-dimensional cell growth confers radioresistance by chromatin density modification. Cancer Res 70: 3925-3934.
60. Le Beyec J, Xu R, Lee SY, Nelson CM, Rizki A, et al. (2007) Cell shape regulates global histone acetylation in human mammary epithelial cells. Exp Cell Res 313: 3066-75.
61. Maynard MA, Ohh M (2007) The role of hypoxia-inducible factors in cancer. Cell Mol Life Sci 64: 2170-2180.
62. Francia G, Green SK, Bocci G, Man S, Emmenegger U, et al. (2005) Down-regulation of DNA mismatch repair proteins in human and murine tumor spheroids: implications for multicellular resistance to alkylating agents. Mol Cancer Ther 4: 1484-1494.
63. Shahrzad S, Bertrand K, Minhas K, Coomber BL (2007) Induction of DNA hypomethylation by tumor hypoxia. Epigenetics 2: 119-125.
64. Chen H, Yan Y, Davidson TL, Shinkai Y, Costa M (2006) Hypoxic stress induces dimethylated histone H3 lysine 9 through histone methyltransferase G9a in mammalian cells. Cancer Res 66: 9009-9016.
65. Wouters BG, Weppler SA, Koritzinsky M, Landuyt W, Nuyts S, et al. (2002) Hypoxia as a target for combined modality treatments. Eur J Cancer 38: 240-257.
66. Ralph SJ, Rodríguez-Enríquez S, Neuzil J, Saavedra E, Moreno-Sánchez R (2010) The causes of cancer revisited: "mitochondrial malignancy" and ROS-induced oncogenic transformation - why mitochondria are targets for cancer therapy. Mol Aspects Med 31: 145-170.
67. Khandrika L, Kumar B, Koul S, Maroni P, Koul HK (2009) Oxidative stress in prostate cancer. Cancer Lett 282: 125-136.
68. Liu SK, Coackley C, Krause M, Jalali F, Chan N, et al. (2008) A novel poly(ADP-ribose) polymerase inhibitor, ABT-888, radiosensitizes malignant human cell lines under hypoxia. Radiother Oncol 88: 258-268.
69. Rappa G, Mercapide J, Anzanello F, Prasmickaite L, Xi Y, et al. (2008) Growth of cancer cell lines under stem cell-like conditions has the potential to unveil therapeutic targets. Exp Cell Res 314: 2110-2122.
70. Miki J, Rhim JS (2008) Prostate cell cultures as in vitro models for the study of normal stem cells and cancer stem cells. Prostate Cancer Prostatic Dis 11:32-39.

Mutation Research 721 (2011) 21–26

Contents lists available at ScienceDirect

Mutation Research/Genetic Toxicology and Environmental Mutagenesis

journal homepage: www.elsevier.com/locate/gentox
Community address: www.elsevier.com/locate/mutres

Application of the DNA adductome approach to assess the DNA-damaging capability of *in vitro* micronucleus test-positive compounds

Kyoko Kato[a], Eiji Yamamura[a], Masanobu Kawanishi[b], Takashi Yagi[b,*], Tomonari Matsuda[c], Akio Sugiyama[a], Yoshifumi Uno[a]

[a] *Safety Research Laboratories, Mitsubishi Tanabe Pharma Corporation, 1-1-1 Kazusakamatari, Kisarazu, Chiba 292-0818, Japan*
[b] *Environmental Genetics Laboratory, Frontier Science Innovation Center, Osaka Prefecture University, 1-2 Gakuen-cho, Sakai, Osaka 599-8570, Japan*
[c] *Research Center for Environmental Quality Management, Kyoto University, 1-2 Yumihama, Otsu, Shiga 520-0811, Japan*

ARTICLE INFO

Article history:
Received 29 July 2010
Received in revised form 4 November 2010
Accepted 28 November 2010
Available online 23 December 2010

Keywords:
Adductome
DNA adduct
In vitro micronucleus test
LC/MS/MS

ABSTRACT

The *in vitro* micronucleus (MN) test is widely used for screening genotoxic compounds, but it often produces false-positive results. To consider the significance of positive results, it is important to know whether DNA adducts are formed in the cells treated with the test compound. Recently, Matsuda et al. developed the DNA adductome approach to detect DNA adducts comprehensively ([4] Kanaly, et al., Antioxid. Redox Signal., 2006, 8, 993–1001). We applied this method to assess the DNA-damaging capability of *in vitro* MN test-positive compounds. CHL/IU cells were treated with compounds from three categories: (1) carcinogens causing DNA alkylation, ethyl methanesulfonate and *N*-methyl-*N'*-nitro-*N*-nitrosoguanidine; (2) carcinogens producing DNA bulky adducts, 2-amino-6-phenyl-1-methylimidazo[4,5-*b*]pyrene, benzo[*a*]pyrene, 7,12-dimethylbenz[*a*]anthracene, and 4-nitroquinoline-1-oxide, and (3) non-carcinogens, caffeine, maltol, and sodium chloride, with or without metabolic activation. With the conditions in which all test compounds gave positive results in the MN tests, DNA was extracted from the cells and hydrolyzed to deoxyribonucleosides, which were subsequently subjected to LC/ESI-MS/MS analysis. All carcinogens (categories 1 and 2) produced various DNA adduct peaks, and some of the *m/z* peak values corresponded to known adducts. No non-carcinogens produced DNA adducts, indicating that these compounds produced MN through different mechanisms from the adduct formation. These results indicate that the adductome approach is useful to demonstrate DNA damage formation of MN test-positive compounds and to understand their mechanisms of action.

1. Introduction

In regulatory science, *in vitro* genotoxicity tests are used for examinations of gene mutations and chromosomal alterations due to DNA damage caused by chemicals. The tests can predict carcinogenic potential of new chemicals applicable as pharmaceuticals, industrial materials, food additives, and cosmetic ingredients. If a compound shows a positive result from these tests, further *in vitro* studies to clarify the mechanism of its action (MOA) or *in vivo* genotoxicity tests are required to assess the risk for human health. Kirkland et al. demonstrated recently that the results from *in vitro* genotoxicity tests, especially the chromosome aberration assay and the micronucleus test in Chinese hamster cells and the mouse lymphoma tk locus assay, are highly discrepant from the results from rodent *in vivo* carcinogenicity tests [1].

Direct or indirect DNA reaction with a compound is an example of MOA, and should be first considered after a positive result is obtained in *in vitro* genotoxicity tests [2]. Direct DNA-reactive compounds are considered to have a non-effective threshold in the dose–response relationship in carcinogenesis; however, non-DNA-reactive (indirect) compounds have a threshold. It is considered that there is no cancer risk below the threshold level exposure; therefore, evidence of direct or indirect reaction of the genotoxicity test-positive compound is important for its cancer risk evaluation. A rapid, sensitive, and accurate method to measure cellular DNA damage, that is, direct DNA reactivity in cells, at the same experimental condition as the genotoxicity test will be required to clarify the MOA of the compound.

DNA damage formation can be measured using various analytical methods [3]. The amount of DNA adducts can be determined by measuring radioactive decay or accelerator mass spectrometry of radiolabeled adduct residues in DNA of the cells treated with radiolabeled chemicals. When the labeled compounds are not available, adducts can be measured by ^{32}P post-labeling analysis, physicochemical methods including mass spectrometry, fluorescence

* Corresponding author. Tel.: +81 72 254 9802; fax: +81 72 254 9938.
E-mail address: yagi-t@riast.osakafu-u.ac.jp (T. Yagi).

1383-5718/$ – see front matter © 2010 Elsevier B.V. All rights reserved.
doi:10.1016/j.mrgentox.2010.11.012

spectrometry, and electrochemical detection, or by immunochemical methods. Each of these approaches has different merits and limitations, and the measurement of DNA adduct formation needs a specific experimental protocol that is dependent on the reactivity and characteristics of each compound. None of these methods is very sensitive and accurate to quantitate the amount of DNA damage at the low concentration used in *in vitro* genotoxicity tests.

Recently, Kanaly et al. developed the "DNA adductome" approach to detect DNA adducts comprehensively using high-performance liquid chromatography equipped with tandem mass spectrometry (LC–MS/MS) [4]. The technique allows comprehensive monitoring of multiple types of DNA adducts that have different molecular weights even though their molecular structures are unknown. The technique can detect adducts in cellular DNA with extremely high sensitivity by comparing the "adductome maps" of treated and untreated cells, and is applicable to the analysis of DNA damage produced in various experimental protocols *in vivo* and *in vitro*.

In this study, we combined this adductome approach with the *in vitro* micronucleus (MN) test to examine whether adductome analysis is useful in regulatory science. Chinese hamster lung (CHL) cells were treated with representative MN-inducing compounds with different MOA, and the increase in the MN incidence was confirmed. Following chemical treatment with the identical condition to the MN test, DNA was extracted from the cells, and DNA adducts were measured by adductome analysis. DNA adducts should not be detected in cells treated with non-DNA-reacting compounds such as caffeine, maltol, and sodium chloride, whereas DNA adducts should be detected in cells treated with directly DNA-reacting compounds such as *N*-methyl-*N'*-nitro-*N*-nitrosoguanidine (MNNG) and 4-nitroquinoline-1-oxide (4-NQO). If the adductome analysis in the MN test condition is valid in this pilot study, newly found MN-positive compounds would be rapidly evaluated in terms of whether they are directly or indirectly reactive to DNA by adductome analysis, which may become a new standard method for the MOA evaluation of *in vitro* genotoxic compounds.

2. Materials and methods

2.1. Test chemicals and reagents

Nine compounds were selected for the MN test and adductome analysis, which were classified into three categories: group A, carcinogens known to produce alkyl residues including ethylmethanesulfonate (EMS) and *N*-methyl-*N'*-nitro-*N*-nitrosoguanidine (MNNG); group B, carcinogens known to make bulky DNA adducts including 2-amino-6-phenyl-1-methylimidazo[4,5-b]pyrene (PhIP), benzo[*a*]pyrene (B[*a*]P), 7,12-dimethylbenz[*a*]anthracene (DMBA), and 4-nitroquinoline-1-oxide (4-NQO), and group C, non-carcinogens including caffeine, maltol, and sodium chloride (NaCl). EMS, B[*a*]P, 4-NQO, and caffeine were purchased from Sigma Co. (St. Louis, MO, USA), and the other chemicals were purchased from Wako Chemical (Osaka, Japan). They were dissolved in distilled water (DW), dimethyl sulfoxide (DMSO), phosphate buffered saline (PBS), physiological saline (saline), or minimum essential medium with 10% calf serum (MEM), immediately before treatment (Table 1). The solvent for each test chemical was used as a negative control. If a chemical required metabolic activation to exert its genotoxicity, rat liver S9 mix, which was designed for the *in vitro* chromosomal aberration test (Kikkoman Corporation, Noda, Japan), was added simultaneously during the treatment period (Table 1).

O^6-methyl deoxyguanosine was purchased from Chemsyn Science Laboratories (Kansas, USA). N^7-methyl deoxyguanosine was synthesized according to the method reported by Yang et al. [5]. [$^{15}N_5$, $^{13}C_{10}$]-2-(2'-deoxyguanosine-8yl)-3-aminobenzanthrone ([$^{15}N_5$, $^{13}C_{10}$]-dG-8-ABA) was kindly supplied by Dr. Takamura of Kanagawa Institute of Technology. These compounds were used for chromatogram standards for the LC/ESI-MS/MS analysis.

2.2. Cells

CHL/IU cells were obtained from DS Pharma Biomedical Co. Ltd. (Osaka, Japan) and used in all experiments. The cells were maintained in Eagle's minimum essential medium (MEM; Nissui Pharmaceutical Co. Ltd., Tokyo, Japan) supplemented with 10% heat-inactivated (56 °C for 30 min) calf serum (CS; Hana-Nesco-Bio Co., Tokyo, Japan) in a 5%-CO_2 incubator at 37 °C.

2.3. MN test

The cells were seeded in ϕ60 mm plastic dishes at 1.6×10^4 cells/dish for the micronucleus tests. The cells were treated with the test chemicals for 6 h in the absence or presence of S9 mix followed by a 20-h recovery period (Fig. 1). Then, the cells were trypsinized and counted. Cytotoxicity was evaluated using the relative cell survival rate, which was defined as the number of chemical-treated cells divided by the number of solvent-treated cells. The cells were spun down and then resuspended in KCl hypotonic solution (75 mM) for 5 min at room temperature. The hypotonized cells were fixed twice in methanol:glacial acetic acid (3:1). Finally, the cells were suspended in methanol containing 1% acetic acid and dropped onto glass slides. After drying, the cells were stained with 0.04% acridine orange solution and subjected to microscopic examination. One thousand intact interphase cells were observed using a microscope, and the incidence of the MN cells was calculated. Fisher's exact test was performed for a statistical analysis.

2.4. DNA extraction

The cells were seeded in ϕ150 mm plastic dishes at 10×10^4 cells/dish for DNA extraction. The cells were treated with test chemicals for 6 h in the absence or presence of S9 mix (Fig. 1). The treatment was carried out with the same experimental protocol as the MN test. The cells were detached by trypsinization, and cellular DNA was extracted according to the method described previously [1]. Purified DNA was suspended in distilled water, and the DNA concentration was determined by measuring absorbance at 260 nm using a UV-vis spectrophotometer. An aliquot of DNA (100 μg) was transferred to a 1.5 mL Eppendorf tube and subjected to evaporation.

2.5. Digestion of DNA samples

DNA was enzymatically hydrolyzed to nucleosides by the micrococcal nuclease/spleen phosphodiesterase (MCN/SPD) method or the nuclease P1 method as described below. In the MCN/SPD method, DNA (100 μg) was enzymatically hydrolyzed to 2'-deoxyribonucleoside-3'-monophosphates for 3 h at 37 °C by the addition of 45 μL of buffer (17 mM sodium succinate and 8 mM $CaCl_2$ at pH 6.0) and 9 μL of MCN/SPD mix consisting of 7.5 units/μL MCN (Worthington Biochemical, Lakewood, NJ) and 0.025 units/μL SPD (Sigma, St. Louis, MO). Then, 3 units of alkaline phosphatase, 30 μL of 0.5 M Tris–HCl (pH 8.5), 15 μL of 20 mM $ZnSO_4$, and 200 μL of water were added and further incubated for 3 h at 37 °C.

In the nuclease P1 method, DNA (100 μg) was enzymatically hydrolyzed to 2'-deoxyribonucleoside-5'-monophosphates by the addition of 300 μL of buffer (30 mM sodium acetate at pH 5.3 and 10 mM 2-mercaptoethanol), 15 μL of 20 mM $ZnSO_4$, 15 μL of water, 3 units of alkaline phosphatase (Wako, Osaka, Japan), and 6 units of nuclease P1 (Wako, Osaka, Japan) for 3 h at 37 °C. Then, 60 μL of 0.5 M Tris–HCl (pH 8.5) was added and incubated for another 3 h at 37 °C.

The digested samples were extracted twice with methanol. The resultant methanol fraction was completely evaporated, and the remaining 2'-deoxyribonucleosides were dissolved in 160 μL of 30% DMSO containing an internal standard (11.5 nM [$^{15}N_5$, $^{13}C_{10}$]-dG-8-ABA).

2.6. Adductome analysis by LC/ESI-MS/MS

The analysis was performed using the Shimadzu HPLC System (Shimadzu), which consists of LC-10ADvp bipumps, a SIL-10ADvp autosampler, a Shim-pack XR-ODS (3.0 mm × 75 mm, 2.2 μm, Shimadzu), and a SPD-10 ADvp UV–Vis detector. The HPLC mobile phases A and B were water and methanol, respectively. The HPLC flow rate was set at 0.2 mL/min. The HPLC gradient started at 5% B, was increased linearly to 80% B over 20 min, and returned to the initial condition over 1 min, which was maintained for a further 10 min. The HPLC system was interfaced with a Quattro Ultima Pt (Waters-Micromass) tandem quadrupole mass spectrometer with an electrospray interface. The temperature of the electrospray source was maintained at 130 °C, and the desolvation temperature was maintained at 380 °C. Nitrogen was used as the desolvation gas (700 L/h), and the cone gas was set to 30 L/h. The capillary voltage was set at 3.5 kV. The collision cell pressure and collision energy were set to 3.8×10^{-3} mBar and 15 eV, respectively. The adducts were analyzed by MS/MS using multiple reaction monitoring (MRM). Ion transition was set at $[M+H]^+ \rightarrow [M+H-116]^+$, the [M+H] of which ranged from *m/z* 250 to *m/z* 702. The LC/ESI-MS/MS was set to monitor 32 ion transitions simultaneously in each injection and 10 μL of each sample was injected 15 times. The ion transitions for an internal standard (*m/z* 526 → *m/z* 405) were monitored in each injection. The absorbance at 254 nm was also monitored with a UV–Vis detector to monitor DNA digestion, and the peak area of 2'-deoxyguanosine (dG) was used for data analysis peak normalization as described below.

2.7. Data analysis

DNA adduct peaks were extracted by comparing chromatograms between the controls (solvent-treated samples) and chemical-treated samples using the following criteria: the signal to noise (S/N) ratio of the detected peak should be more than 3, and the peak area should be 3 times larger than the control peak. When a possible adduct peak was detected, a repeated MN test and adductome analysis were

Table 1
Summary of *in vitro* micronucleus tests.

Chemical	Solvent	Dose (μg/mL)	S9 mix	Cytotoxicity (relative cell survival) (%)	MN frequency (%)[b]	Control MN frequency (%)[b]
EMS	PBS	1000	–	101.0	10.15[c]	1.65[c]
MNNG	DMSO	2	–	98.5	13.25[c]	1.90[c]
PhIP	DMSO	12	+	79.5	16.00[c]	0.75[c]
B[*a*]P	DMSO	10	+	52.5	11.00[c]	1.25[c]
DMBA	DMSO	3	+	69.5	17.50[c]	0.75[c]
4-NQO	DMSO	0.5	–	62.1	5.90[c]	0.70[c]
Caffeine	DW	2000	–	92.7	4.35[c]	0.60[c]
Maltol	Saline	200	–	69.3	4.75[c]	0.55[c]
NaCl	MEM[a]	7500	–	85.2	4.00[c]	0.75[c]

[a] Culture medium (MEM supplemented with 10% CS).
[b] Mean of duplicate culture.
[c] $p < 0.001$ vs. controls by Fisher's exact test.

conducted to confirm reproducibility. The peak area was calculated using Masslynx version 4.0 (Waters) and normalized using the peak areas of dG and the internal standard (I.S.) as described by the following equation: Normalized peak area = (peak area of putative DNA adducts)/(dG area)/(I.S. area) × 10^7.

3. Results

3.1. Induction of micronucleated (MN) cells

The results from *in vitro* micronucleus tests with CHL/IU cells are summarized in Table 1. Since all test compounds are known to induce MN cells with various MOA in the presence or absence of S9-mix, the appropriate experimental conditions were determined in the present experiments. All test compounds induced significantly higher MN incidences (>4.0%) than the corresponding controls (solvents) at the concentrations giving higher than 50% cell survival. The incidence of MN cells in the negative control (solvent) ranged from 0.7 to 1.9%. The carcinogens, PhIP, B[*a*]P, and DMBA, significantly induced MN in the presence of S9-mix ($p < 0.001$), whereas other carcinogens, EMS, MNNG, and 4-NQO, and non-carcinogens, caffeine, maltol, and sodium chloride, induced MN in the absence of S9-mix ($p < 0.001$). These treatment conditions were used for the subsequent comprehensive DNA adductome analysis.

3.2. DNA adductome analysis

In the LC–MS/MS chromatograms of all samples derived from the cells treated with the 6 test carcinogens (groups A and B), putative DNA adduct peaks were detected. The detected peak molecular ion (*m/z*), retention times, normalized peak areas, and identified or presumed DNA adducts obtained from the chromatograms are summarized in Table 2. Among the test carcinogens, most adduct peaks were detected by both digestion methods; however, the PhIP-8-dG adduct was detected only by the nuclease P1 method, and the B[*a*]P and DMBA-induced DNA adducts were detected only by the MCN/SPD method. Non-carcinogens(group C) yielded no DNA adduct peaks, even under the conditions that showed positive results in the MN tests. The possible structures of some DNA adducts were estimated from their *m/z* according to the findings of previous reports (Fig. 2).

A representative chromatogram of *N*-methyl-*N*′-nitro-*N*-nitrosoguanidine (MNNG)-treated samples is shown in Fig. S1. Two peaks at *m/z* 282 corresponding to the molecular ion of methylated dG were detected in the MNNG-treated samples. The first peak (retention time: 7.6 min) was identified as N^7-methyl-2′-deoxyguanosine (N^7-methyl-dG), and the second peak (retention time: 13.7 min) was identified as O^6-methyl-2′-deoxyguanosine (O^6-methyl-dG) by comparison with the chromatograms of each standard substance.

For ethylmethanesulfonate (EMS), two peaks at *m/z* 296 were detected (Fig. S2), and the molecular ion corresponded to ethylated dG. The first and second peaks were thought to be N^7-ethyl-2′-deoxyguanosine (N^7-ethyl-dG) and O^6-ethyl-2′deoxyguanosine (O^6-ethyl-dG), respectively, because the amount and polarity of N^7-ethyl-dG would be higher than those of O^6-ethyl-dG [6].

For 2-amino-6-phenyl-1-methylimidazo[4,5-b]pyrene (PhIP), the peaks at *m/z* 450 and 490 were detected (Figs. S3 and S4), and the *m/z* 490 corresponded to *N*-(deoxyguanosin-8-yl)-PhIP (PhIP-8-dG).

For benzo[*a*]pyrene (B[*a*]P), two peaks at *m/z* 570 were detected (Fig. S5). These peaks were considered to be 10-(deoxyguanosine-N^2-yl)-7,8,9-trihydroxy-7,8,9,10-tetrahydrobenzo[*a*]pyrene (B[*a*]P-DE-N^2-dG).

For 7,12-dimethylbenz[*a*]anthracene (DMBA), 12 possible DNA adducts were detected (Figs. S6–S12).

For 4-nitroquinoline-1-oxide (4-NQO), several peaks were detected (Fig. S13–S16). The *m/z* 410 corresponded to 3-(deoxyadenosin-N^6-yl)-4-aminoquinoline 1-oxide (4-AQO-N^6-dA), and *m/z* 426 corresponded to 3-(deoxyguanosine-N^2-yl)-4-aminoquinoline 1-oxide (4-AQO-N^2-dG) and *N*-(deoxyguanosine-8-yl)-4-aminoquinoline 1-oxide (4-AQO-8-dG).

All adduct peaks with their *m/z*, retention times, and peak areas are illustrated in the adductome maps (Fig. 3).

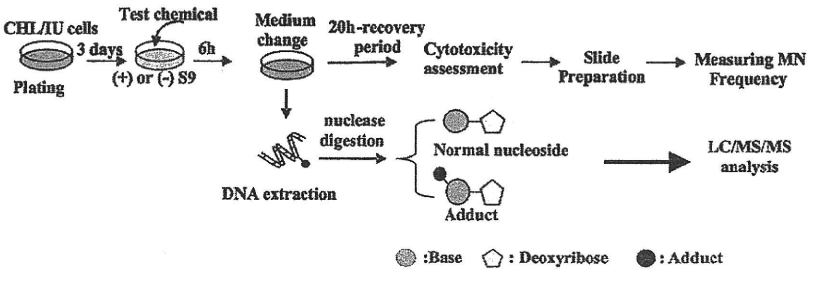

Fig. 1. Schematic outline of the *in vitro* MN test and adductome analysis.

Table 2
Summary of adductome analysis.

Group	Chemical	Peak no.	*m/z*	RT (min)	Normalized peak area		Identified or presumed adducts
					MCN/SPD method	NucleaseP1 method	
A	MNNG	1	282	7.6	2163	2240	N^7-methyl-dG*
		2		13.7	157	158	O^6-methyl-dG*
	EMS	1	296	9.6	2994	5816	N^7-ethyl-dG
		2		16.0	33	235	O^6-ethyl-dG
B	PhIP	1	450	19.1	N.D.	5	–
		2	490	19.6	N.D.	16	PhIP-dG
	B[*a*]P	1	570	22.1	2	N.D.	B[*a*]P-DE-N^2-dG
		2		22.5	6	N.D.	
	DMBA	1	558	24.6	3	N.D.	DMBA-DE-dA
		2	572	19.3	8	N.D.	–
		3		21.4	10	N.D.	–
		4	574	19.3	5	N.D.	DMBA-DE-dG
		5		22S.7	13	N.D.	
		6		23.5	25	N.D.	
		7	590	17.6	12	N.D.	–
		8		18.1	17	N.D.	
		9	596	23.5	5	N.D.	Sodium adducts of No.6
		10	606	18.7	14	N.D.	–
		11		20.7	3	N.D.	–
		12	612	19.3	4	N.D.	–
	4NQO	1	371	14.2	7	4	–
		2	410	12.3	155	112	4-AQO-N^6-dA
		3		17.3	N.D.	6	
		4	426	14.2	4	3	4-AQO-N^2-dG or 4-AQO-8-dG
		5		14.7	4	24	
		6	456	14.6	4	12	–
C	Caffeine Maltol NaCl	No specific peak was detected					

"N.D." means "not detected". "–" represents unknown adduct.
Adducts with and without asterisk show "identified" and "presumed" adducts, respectively.

4. Discussion

In this study, we used the adductome approach to detect the DNA damage caused by the compounds that gave positive results in the MN test condition. Three categories of compounds with different MOA for MN induction were selected. All tested carcinogens were confirmed to form DNA adducts; in contrast, three non-carcinogens yielded no DNA adduct peaks.

In the group A compounds consisting of DNA alkylating agents, O^6- and N^7-methyl-dG and O^6- and N^7-ethyl-dG were detected in the MNNG- and EMS-treated cells, respectively. Although N^3-methyl-dA and N^3-ethyl-dG have been found in other chromatographic analyses [6,7], these adducts were not detected in this adductome analysis, which was probably due to their instability. Another minor lesion, 1-methyl dG, was not detected because its amount was considered to be lower than the detection limit. These results indicate that alkylation of O^6 and N^7 positions of dG would be proof of DNA damage by the group A compounds in the MN-positive experimental condition.

In the group B compounds producing DNA bulky adducts, each compound yielded at least two DNA adduct peaks in the adductome analysis. PhIP yielded two peaks at *m/z* 450 and 490; the former peak is one of unidentified minor adducts [8], but the latter peak is coincident with PhIP-8-dG, the major adduct formed through a reactive intermediate *N*-acetoxy-PhIP [8]. B[*a*]P yielded two peaks at *m/z* 570, which are coincident with the molecular ions of the major adducts B[*a*]P-DE-N^2-dG consisting of four types of stereoisomers [9]. DMBA yielded twelve possible adduct peaks, which agrees with the report showing at least eight DNA adducts induced by DMBA with the ^{32}P-post-labeling analysis [11]. Three DMBA-induced peaks at *m/z* 574 would be stereoisomers of the DMBA-dG adduct, and a peak at *m/z* 558 is coincident with the molecular ion of DMBA-dA, but other peaks are unknown adducts. Six possible DNA adduct peaks were detected in the 4-NQO-treated cellular DNA. Two peaks at *m/z* 410 and 426 correspond to 4-AQO-dG and 4-AQO-dA adducts, respectively, in which several types of 4-NQO binding to C8, N^2, and N^6 of dG and dA are included [12–15], and other peaks cannot be identified because 4-NQO produces various base lesions with different half-life periods [16,17]. These results indicate that the adductome analysis can detect various types of DNA bulky adducts that were identified with the existing methods by other investigators. The efficiency of the adduct peak detection is different between nuclease P1 and MCN/SPD digestion methods in each compound because their enzyme activities on adducted-base excision would vary dependent on the adduct structures. The use of both digestion methods is necessary to detect DNA adducts when new chemicals are tested.

None of the group C compounds, caffeine, maltol, and sodium chloride, which are non-carcinogens but known to produce MN, yielded adduct peaks. Caffeine may interact with DNA repair enzymes and/or nucleotide precursor pools [19], and shows positive results in various genotoxicity tests [18]. Despite a great number of investigations over the past 50 years, the MOA of these compounds is not well understood. The cytotoxic effect of maltol can be explained by its pro-oxidant properties; the maltol/metal complex generates reactive oxygen species (ROS) causing the production of hydroxyl radicals and leading to the formation of DNA base adducts [20]. However, no ROS-related DNA adducts were detected in the present analysis. Sodium chloride increased the incidence of MN cells at extremely high concentrations (c.a. 128 mM). Hyperosmotic medium can cause chromosomal aberrations in CHO cells, mutations at the TK locus in L5178Y mouse lymphoma cells, and at the HPRT locus in V79 cells [21]. However, the mechanisms by which abnormalities are induced in cells subjected to high osmotic pressure are unknown. Although the failure to detect DNA adducts with the non-carcinogens does not mean necessarily that DNA adducts were not formed, DNA adductome is the promising